UNIVERSITAT POLITÈCNICA
DE CATALUNYA

Modelling the electrostatic actuation of MEMS: state of the art 2005.

A. Fargas Marquès, R. Costa Castelló and A.M. Shkel

IOC-DT-P-2005-18
Setembre 2005

Institut d'Organització i Control
de Sistemes Industrials

MODELING THE ELECTROSTATIC ACTUATION OF MEMS. STATE OF THE ART 2005

A. Fargas Marquès*, R. Costa Castelló*, and A. M. Shkel+
*Institut d'Organització i Control de Sistemes Industrials, IOC-UPC and
+University of California at Irvine

July 2005

Abstract

Most of MEMS devices are actuated using electrostatic forces. Parallel or lateral plate actuators are the types commonly used. Nevertheless, electrostatic actuation has some limitations due to its non-linear nature. This work presents a methodic overview of the existing techniques applied to the Micro-Electro-Mechanical Systems (MEMS) electrostatic actuation modeling and their implications to the dynamic behavior of the electromechanical system.

1 Introduction

The field of Micro-Electro-Mechanical Systems (MEMS) has undergone a startling revolution in recent years. It is now possible to produce accelerometers less than one millimeter on a side, functioning motors that can only be seen with the aid of a microscope, gears smaller than a human hair, and needles so tiny they can deliver an injection without stimulating nerve cells.

The use of existing integrated circuit technology in the design and production of MEMS devices allows these devices to be batch-manufactured, what in turn converts them due to their quantity in almost inexpensive. The first sector to benefit from this revolution has been the automotive industry, where devices and applications that once could only be dreamed about have suddenly been made possible and are used everywhere.

The ability to manufacture mechanical parts such as resonators, sensors, gears and levers on a micron length scale is not however the end of the story. The challenge is also to understand and control the physical systems behavior on these scales. That is, an understanding of fluid, electromagnetic, thermal, and mechanical forces on the micron length scale is necessary in order to understand the operation and function of MEMS devices.

In this framework, the methods of actuation and sensing of this new devices have been a critically important topic over the years. There is not a perfect method, and the decision usually depends on the actual device and the specifications of the system.

The main actuation and sensing properties used in MEMS are

- Piezoresistivity: When a piezoresistive material is stressed, it reduces or increases its ability to transport current. Using this property, movement can be measured as a current difference between the two extremes of a deformed piezoresistive material.

Table 1: Comparison between actuation/sensing methods [Kovacs, 1998]

	Parameter	Local circuits	DC response	Complex	Linearity	Issues
Piezoresistive	strain	NO	YES	+	+++	High temperature dependance Easy yo integrate
Piezoelectric	force	NO	NO	++	++	High sensitivity Fabrication complex
Electrostatic	displacement	YES	YES	++	poor	Very simple Low temperature coefficients
Thermal	strain	NO	YES	+	poor	Cooling problems Interference with electronics
Magnetic	displacement	NO	YES	+++	+	Very complex Post fabrication
Optical	displacement	NO	YES	+++	+++	Difficult to implement

- Piezoelectricity: Piezoelectric materials deform under the influence of a voltage bias, or reciprocally, under deformation generate a polarization between their extremes. Using this relationship, movement can be controlled or sensed.

- Electrostatics: The polarization between two plates generates an electrostatic force between them. This fact can be used to actuate the device. On the other hand, relative movement of two polarized plates generates an induced current that can be sensed, and the movement is proportional to the current.

- Thermal: Deformation of the materials due to thermal effects can be used to actuate devices, forcing the increase of temperature in the device. A typical way of achieving the temperature increase is feeding a high current through a conducting material and using the Joule effect.

- Electromagnetism: Magnetic fields generated by a current flowing through an spiral can be used to actuate magnetic materials. Similarly, induced current can be used to sense movement of a magnet.

- Optics: Reflectivity, transparency, 'admissibility' of the materials can be used to sense and actuate devices with the help of a light source and a light sensor. The diffraction of the light in a gap, the light patterns of the light through a device, the reflected light in a mirror can be used to extract movement or to induce movement to a MEMS device. Usually, the light source would be a LED or would be carried by an optic fiber.

All of them have their advantages and drawbacks (Table 1 and Figure 1), and they are basically related to the selected fabrication method. (See a comparison in [Burns et al., 1995])

Piezoresistive sensing is a common method in engineering to measure strain and displacements. Metal strain gauges are used extensively in engineering. The same principles have been used with semiconductors, and the case apply to doped-silicon or the different layers of material that can be deposited in MEMS (SiO_2, Al_2O_3). Piezoresistive sensing is easy to integrate, and many viable applications exist [Chui et al., 1998], [Tortonese et al., 1993]. However, its temperature dependance and fabrication stresses calibration reduce its market share [Lee, 1997].

Piezoelectric materials are used for actuation and sensing, but the sensing is limited due to their lack of a DC response. Their properties are well known, and have been used for decades. Most of the first sensors used piezoelectric actuation, and it is still used nowadays. However, their high temperature sensitivity, nonlinear working zones and hysteresis prevent from using them more often. When using silicon-based sensors, post-processing is needed to deposit the material. ZnO or PVDF are typical materials used nowadays. Examples of piezoelectric applications could be beam

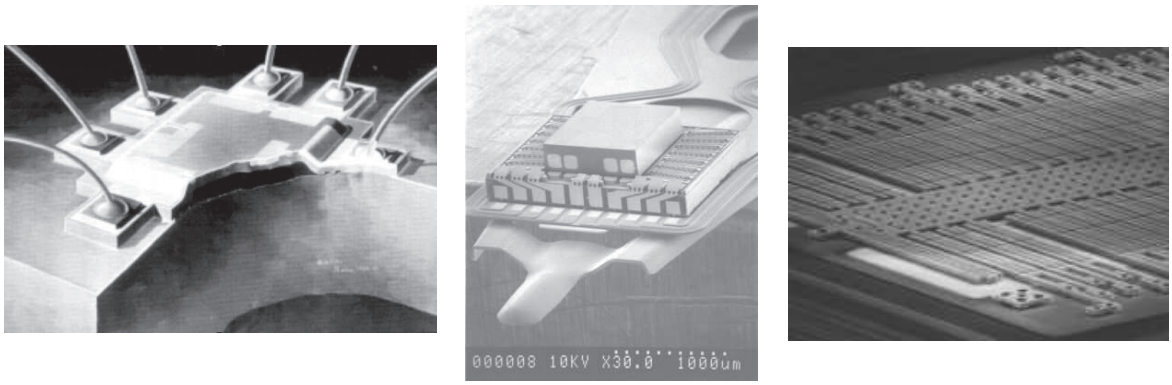

Figure 1: Piezoresistive pressure sensor. Piezoelectric micro-positioner. Analog Devices ADXL150's electrostatic accelerometer

actuation and sensing [Gaucher et al., 1998] and actuation in microscopy [Itoh et al., 1996], [Minne et al., 1995].

Thermal actuation and sensing relays on the use of the thermal deformations of the materials that are used to build the device. The method is easy to implement, and there exist some working devices using this phenomena [Huang and Lee, 2000], [Robert et al., 2003], [Oz and Fedder, 2003]. However, the difficulty of isolating the temperature changes to a fixed area, and the possible interferences with control electronics or other thermally dependent elements, prevents from using this method. [Jonsmann et al., 1999]

Magnetic actuation is a common method in the macroworld, however, it is no easily scaled to the MEMS devices. The main problem is the reduction of the achievable forces in a factor of ten thousand when the sizes are reduced by a factor of ten [Niarchos, 2003]. This fact, combined with the constructive difficulties, leaves magnetic actuation application limited. However, successful examples of application exist in the literature, as it could be in gyros [Dauwalter and Ha, 2004], [M Hashimoto and Esashi, 1995] or relays [Tilmans et al., 1999].

Optical actuation and sensing is a desirable method, due to its non-interfering technology. However, although some working devices exist [Lethbridge et al., 1993], [Zook et al., 1995] there are considerable challenges for mass fabrication. The necessity of integrating a light source, building reflecting surfaces and aligning the whole set-up, is time demanding and no batch-fabrication implementation exist.

All these problems leave electrostatic actuation and sensing as a really desirable method.

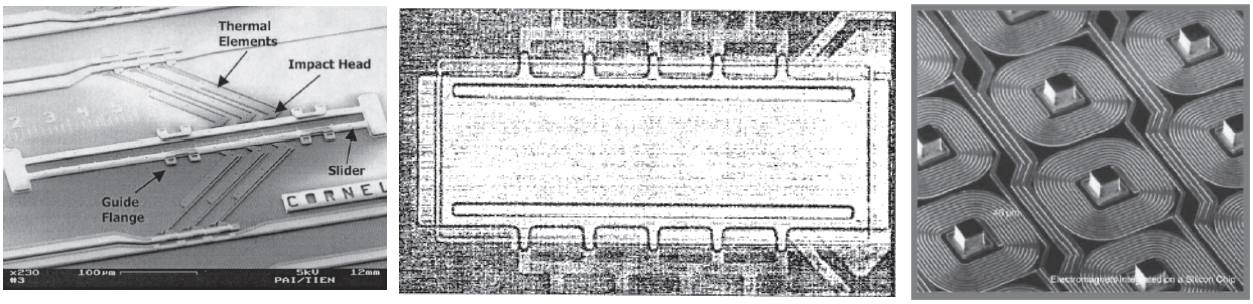

Figure 2: Thermal vibromotor [Pai and Tien, 2000]. Optically excited microbeam [Zook et al., 1995]. Micromachined Cu coils [Niarchos, 2003].

Building a capacitor, with the existing fabrication methods is straightforward. One must put together two parallel surfaces and then apply potential difference between the two parts to obtain a good actuator or sensor. This simplicity has made electrostatic actuation and sensing ubiquitous. One can find it in the first MEMS designs to build a gate transistor [Newell, 1968]. Nowadays, capacitive effects are used in resonators [Attia et al., 1998], accelerometers [Kuehnel, 1995], [Brosnihan et al., 1995], optical switches [Juneau et al., 2003], [Sane and Yazdi, 2003], micro-grippers [Chu et al., 1996], micro force gauges [Roessig, 1995], micro-pumps [Teymoori and Abbaspour-Sani, 2002], gyroscopes [Juneau, 1997], [Kranz et al., 2003], pressure sensors [Gupta and Senturia, 1997], RF switches [Huang et al., 2003], and microscopy [Blanc et al., 1996], [Shiba et al., 1998].

Even though practically and economically attractive, capacitive actuation has its own trade-offs and challenges. On-chip amplification is usually needed for capacitive sensing, due to the femptofarad measure that must be achieved. Parasitic capacitances can affect the final read-out. And finally, although large forces can be generated, they can be heavily non-linear.

Consequently, the good understanding of the phenomenons that take place is essential to obtain a high performance device with electrostatic actuation and sensing. And this is more relevant given the increasing number of new devices that are continuously designed using these methods of actuation and sensing.

2 Problem Description

A basic building block of any electrostatically driven or sensed device is a microbeam. It forms one side of a variable capacity air gap capacitor. Opposite to the microbeam lays the driving or sensing electrode that completes the capacitor.

If a voltage is applied to the electrode, a force is generated on the beam that deflects under this action. Alternatively, if the capacitance changes due to a deflection of the microbeam, the charge redistribution and resulting flow of current can be detected. Examples of the typical configurations are shown in Figure 3.

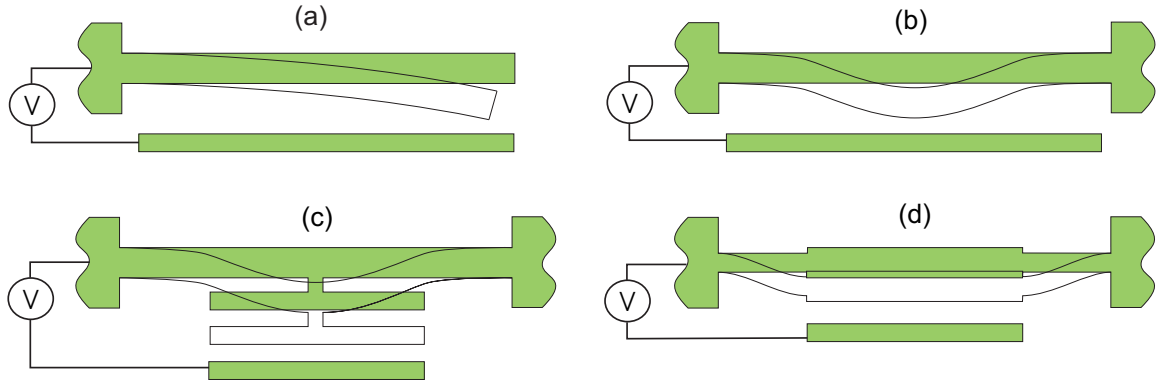

Figure 3: Basic MEMS capacitor configurations (a) Free-end beam. The beam bends under the action of the force. The gap, and consequently the force, is not uniform. Maximum bending at the end. (b) Clamped-clamped beam. The beam bends forming a not uniform gap. Force variable depending on position. Maximum bending in the center. (c) Clamped-clamped beam. A parallel plate added to maintain the gap uniform. Maximum bending in the center which defines the capacitor gap. (d) Guided-end beam. Gap and force uniform. Maximum bending at the extreme of both suspension-beams.

When the goal is sensing displacement, a DC polarization voltage is applied to the capacitor, and the generated current is usually detected with a transresistance amplifier [Roessig, 1998]. More sophisticated sensing schemes can also be used to improve the detection. This includes complex electronics designs based on impedance, capacitive or source/drain pick-off [Burstein, 1995]. Charge detection schemes has also been investigated [Seeger and Boser, 2003].

When the goal is driving the beam, an electric load is applied to the microbeam. Depending on the nature of the device, the electric load is composed of a DC polarization voltage and, sometimes, an AC component designed to excite harmonic motions.

DC polarization is used to achieve permanent displacements of the beam. Moving optical switches, adjusting elements, closing gate transistors, moving valves or acting micro-grippers are typical applications.

However, in most cases, resonant devices are used. In that case, an AC component is added to the driving voltage to excite the harmonic motions of the beam.

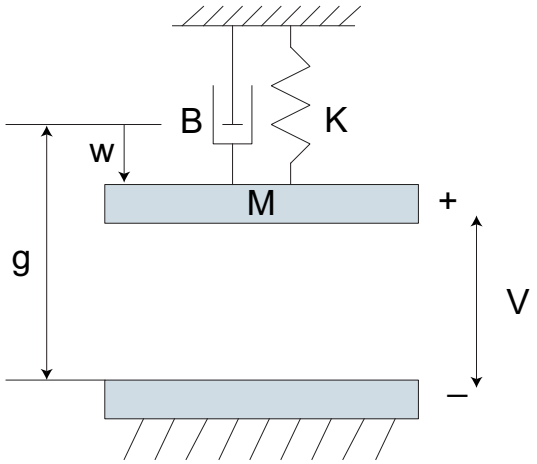

Figure 4: Scheme of a parallel plate actuator

Figure 4 shows the simplified lumped mass-spring system model of a MEMS device with a parallel plate actuator. To understand the phenomena, one can turn to the energy of the electromechanical system

$$T = \frac{1}{2}\mathrm{M}\ \dot{\hat{w}}^2;\ U_k = \frac{1}{2}\mathrm{K}\ \hat{w}^2;\ U_e = -\frac{1}{2}\frac{\varepsilon_0\,\mathrm{A}_c}{(\mathrm{g}-\hat{w})}V^2 \tag{1}$$

$$E = T + U_k + U_e \tag{2}$$

where $\hat{w}$ is the displacement of the moving plate from its initial equilibrium, T is the kinetic energy of the plate, U_k is the potential energy stored in the spring, U_e is the potential energy stored in the parallel plate capacitor, and E the energy of the whole system.

The dynamics of the system is derived as follows, using Lagrange's formulation,

$$\frac{d}{dt}\left(\frac{\partial L}{\partial \dot{\hat{w}}}\right) - \frac{\partial L}{\partial \hat{w}} = \frac{\partial W}{\partial \hat{w}} \tag{3}$$

being $L = T - U_k - U_e$ the Lagrangian of the system, and introducing the damping force, $F_d = -\mathrm{B}\ \dot{\hat{w}}$ as the only contributing force to the work (W) of the system

$$\mathrm{M}\ \ddot{\hat{w}} + \mathrm{K}\ \hat{w} - \frac{1}{2}\frac{\varepsilon_0\,\mathrm{A}_c}{(\mathrm{g}-\hat{w})^2}V^2 = -\mathrm{B}\ \dot{\hat{w}} \tag{4}$$

This equation is the usual mass-spring-damper equation of dynamics.

From this formulation, the force generated between the parallel plates, using basic electrostatics, takes the following form

$$F = \frac{1}{2}\frac{\varepsilon_0 \, \mathrm{A}_c}{(\mathrm{g} - \hat{w})^2} V^2 \tag{5}$$

where ε_0 is the dielectric constant, g is the initial gap between the plates, A_c is the area of the plates and V is the applied voltage between the electrodes. As it can be observed, this force is inversely proportional to the gap between the plates of the actuator. As the gap decreases, the generated attractive force increases quadratically. The only opposing force to the electrostatic loading is the mechanical restoring force (K).

If the voltage is increased, the gap decreases generating an incremented force. At some point the mechanical forces defined by the spring cannot balance this force anymore. Once reached this state, the electrodes will snap one against the other, and in most cases, the system would be permanently disabled.

Consequently, the electrostatic loading has an upper limit beyond which the mechanical force can no longer resist the opposing electrostatic force, thereby leading to the collapse of the structure. This actuation instability phenomenon is known as pull-in, and the associated critical voltage is called the *Pull-in Voltage*.

Several studies have investigated this behavior of microbeams under various loading conditions. The earliest such study may be found in the pioneering work of Nathanson et al. [Nathanson et al., 1967] [Newell, 1968]. In their study of a resonant gate transistor they constructed and analyzed the mass-spring model of electrostatic actuation. They predicted and offered the first theoretical explanation of the so-called pull-in instability.

Since then, numerous investigators have analyzed mathematical models of electrostatic actuation in attempts to further understand and control the pull-in instability. Despite more than three decades of work in the area of electrostatically actuated MEMS, the complete dynamics of the electrostatic-elastic system is relatively unexplored.

There are a lot of aspects to be clarified. Some studies just center their goal in the immediate application of the sensor, and a simple mass-spring model can approximate the basic dynamics. However, these kind of models cannot predict the inherent nonlinearities of the electrostatic force and the beam deformation ([Chu et al., 1996], [Castañer and Senturia, 1999]).

Other approaches rely on the partial differential equations linearized around the working point. Using this formulation, better results are achieved, but the dynamics only apply for small deflections [Ijntema and Tilmans, 1992].

Other studies analyze the response of a microbeam to a generalized transverse excitation and with axial force using Rayleigh's energy method to approximate the fundamental natural frequency of the straight, undeflected beam [Tilmans and Legtenberg, 1994].

Recently, some authors have used the nonlinear equation representing the idealized electrostatic structure to analyze the behavior ([Flores et al., 2003], [Abdel-Rahman et al., 2002]).

However, no unified formulation of the problem has been offered. Questions about where, when, and how touchdown occurs are still to be answered. And this knowledge is essential to design and implement the correct control of the new generation of high performance and self-calibrated MEMS devices.

3 Model Formulation

In this section, the complete idealized model of an electrostatically actuated beam is presented. This model englobes the main characteristics that can be found in a large number of MEMS devices which rely on electrostatic actuation.

The analysis of the different participating terms is presented separately, to address each aspect of the dynamics. Finally, the complete formulation is presented together.

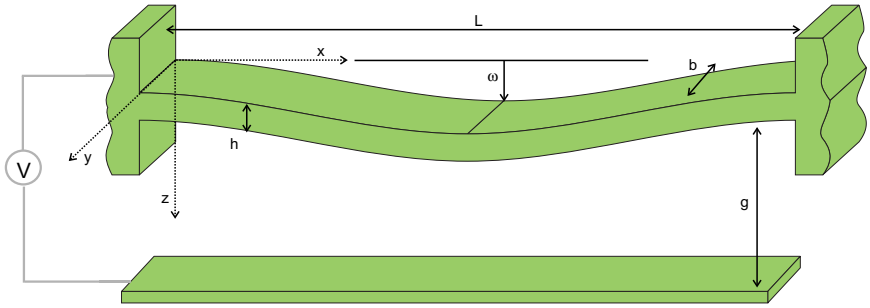

Figure 5: Basic scheme of a deflected beam

3.1 Mechanical model

In MEMS devices, we have a basic structure: the *beam*. This mechanical component, and its extension, the *plate*, generate the majority of MEMS sensors and actuators. Consequently, the first step to analyze the behavior of any device is to understand and model the dynamic characteristics of a beam.

The deformation of a beam (Figure 5), using the Euler-Bernouilli theory of thin beams [Rao, 1990] is composed of two basic terms [Younis and Nayfeh, 2003], the potential energy generated due to the deformation of the beam

$$U_{def} = \frac{\mathrm{EI}}{2} \int_0^{\mathrm{L}} \left(\frac{\partial^2 \hat{w}}{\partial \hat{x}^2} \right)^2 \mathrm{d}\hat{x} \tag{6}$$

that it's proportional to its curvature, $\frac{\partial^2 \hat{w}}{\partial \hat{x}^2}$, and the kinetic energy due to its movement

$$T = \frac{\rho \mathrm{bh}}{2} \int_0^{\mathrm{L}} \left(\frac{\partial \hat{w}}{\partial \hat{t}} \right)^2 \mathrm{d}\hat{x} \tag{7}$$

where $\hat{w}$ is the oscillation amplitude, ρ is the density of the beam, b and h are the width and height of the section of the beam, L is the longitude of the beam, E is the Young Modulus and I is the moment of inertia of the cross-section.

Typically in MEMS, a beam can also be externally stretched by an axial force $\hat{N}(\hat{t})$ (Figure 6). This force could be generated by different sources: thermal load, fabrication stresses, external beam tuning, etc. In this case, another energy term appears that englobes the deformation generated by the external force

$$U_N = \frac{\hat{N}(\hat{t})}{2} \int_0^{\mathrm{L}} \left(\frac{\partial \hat{w}}{\partial \hat{x}} \right)^2 \mathrm{d}\hat{x} \tag{8}$$

As can be observed, the deformation is proportional to the axial force.

Finally, in the case of large oscillations, the beam movement generates self-stretching forces that actuate as structural damping. This effect can be accounted assuming that an internal force, P,

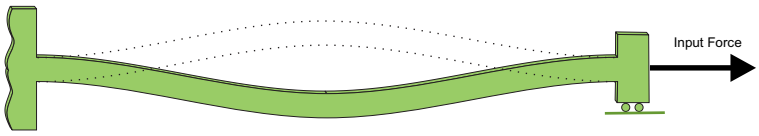

Figure 6: Vibrating beam oscillating under the influence of an axial force

is producing an elongation of the beam. This force would have the following form [Rao and Raju, 2003], [Roessig, 1998]

$$P = \frac{\mathrm{bhE}}{4\mathrm{L}} \int_0^{\mathrm{L}} \left(\frac{\partial \hat{w}}{\partial \hat{x}} \right)^2 \mathrm{d}\hat{x} \tag{9}$$

and, substituting this force in (8), we obtain the energy of deformation due to self-stretching [Younis and Nayfeh, 2003]

$$U_{int} = \frac{\mathrm{bhE}}{8\mathrm{L}} \left[\int_0^{\mathrm{L}} \left(\frac{\partial \hat{w}}{\partial \hat{x}} \right)^2 \mathrm{d}\hat{x} \right]^2 \tag{10}$$

The dynamic equation of the free deflection of an homogeneous beam undergoing bending can be obtained using the Lagrange equations, from the Lagrangian

$$L = T - U_{def} - U_N - U_{int} \tag{11}$$

and it is written as follows

$$\mathrm{E'I}\frac{\partial^4 \hat{w}}{\partial \hat{x}^4} + \rho \mathrm{A}\frac{\partial^2 \hat{w}}{\partial \hat{t}^2} - \left[\hat{N}(\hat{t}) + \frac{\mathrm{E'A}}{2\mathrm{L}} \int_0^{\mathrm{L}} \left(\frac{\partial \hat{w}}{\partial \hat{x}} \right)^2 \mathrm{d}\hat{x} \right] \frac{\partial^2 \hat{w}}{\partial \hat{x}^2} = 0 \tag{12}$$

where A = bh is the area of the section of the beam, and in this case, the extended Young Modulus, E' = E$/(1-\nu^2)$, is introduced to account for a wide microbeam (plate) where ν is the Poisson ratio. For a narrow beam E' = E.

As can be observed, the microbeam dynamics is composed of four terms: the beam resistance to bending, the inertia due to movement, the beam stiffness due to the externally applied axial load and mid-plane stretching due to elongation of the beam. The first three components are treated as linear terms in the equation of motion, whereas the third component is represented by a nonlinear term in the equation of motion.

For convenience, and uniformity with other formulations, we introduce the following nondimensional variables

$$w = \frac{\hat{w}}{\mathrm{g}},\ x = \frac{\hat{x}}{\mathrm{L}},\ t = \frac{\hat{t}}{\mathrm{T}} \tag{13}$$

where T is a time-scale defined as T = $(\rho \mathrm{bhL}^4/(\mathrm{E'I}))^{1/2}$. Writing down the equation in the non-dimensional variables

$$\frac{\partial^4 w}{\partial x^4} + \frac{\partial^2 w}{\partial t^2} - \left[\alpha_1 \Gamma(w, w) + N \right] \frac{\partial^2 w}{\partial x^2} = 0 \tag{14}$$

The parameters appearing in equation (14) can be defined as follows

$$\alpha_1 = 6 \left(\frac{\mathrm{g}}{\mathrm{h}} \right)^2,\ N = \frac{\hat{N}\mathrm{L}^2}{\mathrm{E'I}} \tag{15}$$

and the operator Γ is defined as

$$\Gamma(f_1(x,t), f_2(x,t)) = \int_0^1 \frac{\partial f_1}{\partial x} \frac{\partial f_2}{\partial x}\, \mathrm{d}x$$

being f_1 and f_2 any two functions of x and t.

Solving of the equations can be done numerically. However, to analyze the oscillation of the beam, the partial differential formulation is usually simplified. One of the most common approaches is to break down the partial differential equations into single-degree of freedom ordinary equations, one for each mode of oscillation. The description of the output is presented as it will be used in the following sections.

Assuming that beam response is composed of an infinite number of oscillation modes, the displacement $\hat{w}$ can be decomposed in

$$\hat{w}(\hat{x},\hat{t}) = \sum_i \hat{q}_i(\hat{t})\hat{\phi}_i(\hat{x}) \tag{16}$$

where $\hat{q}_i(\hat{t})$ is the time-dependent modal displacement for the oscillation mode i and $\hat{\phi}_i(\hat{x})$ is the position-dependent modal shape. Substituting (16) in the equations of the potential energy of the system and rearranging terms a spring-equivalent equation can be obtained [Roessig, 1998]

$$\begin{gathered} U_i = U_{def,i} + U_{N,i} + U_{int,i} = \\ \left[\frac{\mathrm{EI}}{2}\int_0^{\mathrm{L}}\left(\frac{\partial^2\hat{\phi}_i}{\partial\hat{x}^2}\right)^2 \mathrm{d}\hat{x} + \frac{\hat{N}(\hat{t})}{2}\int_0^{\mathrm{L}}\left(\frac{\partial\hat{\phi}_i}{\partial\hat{x}}\right)^2 \mathrm{d}\hat{x}\right]\hat{q}_i^2 + \frac{\mathrm{bhE}}{8\mathrm{L}}\left[\int_0^{\mathrm{L}}\left(\frac{\partial\hat{\phi}_i}{\partial\hat{x}}\right)^2 \mathrm{d}\hat{x}\right]^2\hat{q}_i^4 = \\ \frac{1}{2}K_{eff,i}\cdot\hat{q}_i^2 + \frac{1}{4}K_{3,eff,i}\cdot\hat{q}_i^4 \end{gathered} \tag{17}$$

And the same can be done for the kinetic energy

$$T_i = \frac{\rho\mathrm{bh}}{2}\int_0^{\mathrm{L}}\hat{\phi}_i^2\mathrm{d}\hat{x}\;\frac{\partial^2\hat{q}_i}{\partial\hat{t}^2} = \frac{1}{2}M_{eff,i}\cdot\ddot{\hat{q}}_i^2 \tag{18}$$

where $(\dot{})$ denotes time-derivative. And using the Lagrange formulation, the oscillation of each of the infinite modes is governed by

$$M_{eff,i}\cdot\ddot{\hat{q}}_i + K_{eff,i}\cdot\hat{q}_i + K_{3,eff,i}\cdot\hat{q}_i^3 = 0 \tag{19}$$

where

$$M_{eff,i} = \rho\mathrm{bh}\int_0^{\mathrm{L}}\hat{\phi}_i^2\mathrm{d}\hat{x} \tag{20}$$

$$K_{eff,i} = \mathrm{EI}\int_0^{\mathrm{L}}\left(\frac{\partial^2\hat{\phi}_i}{\partial\hat{x}^2}\right)^2\mathrm{d}\hat{x} + \hat{N}(\hat{t})\int_0^{\mathrm{L}}\left(\frac{\partial\hat{\phi}_i}{\partial\hat{x}}\right)^2\mathrm{d}\hat{x} \tag{21}$$

$$K_{3,eff,i} = \frac{\mathrm{bhE}}{2\mathrm{L}}\left[\int_0^{\mathrm{L}}\left(\frac{\partial\hat{\phi}_i}{\partial\hat{x}}\right)^2\mathrm{d}\hat{x}\right]^2 \tag{22}$$

Using this approach, the behavior of the beam, for a given mode of vibration, can be approximated by a mass-spring model, allowing to use known analysis techniques.

3.2 Electrostatic Actuation

In MEMS, the basic electrostatic system is a parallel-plates capacitor (Figure 7). In this case, electrostatic forces are generated between two conducting elements separated a distance g by a dielectric element. In MEMS, the dielectric is usually air. And an usual assumption is that the distance g is differentially uniform between the two plates.

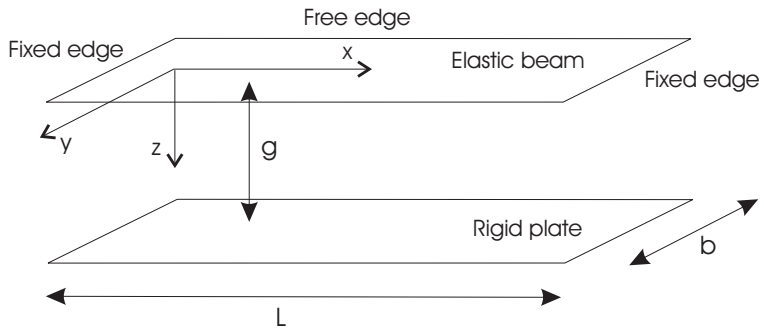

Figure 7: Geometry of the idealized capacitor [Pelesko and Triolo, 2001]

Having these assumptions in mind, the electrostatic field ϕ between the plates of a capacitor (Figure 7) satisfies

$$\nabla^2\phi = 0, \tag{23}$$

$$\phi(\hat{x}, \hat{y}, \mathrm{g}) = 0, \quad \hat{x}\epsilon[-\mathrm{L}/2, \mathrm{L}/2], \quad \hat{y}\epsilon[-\mathrm{b}/2, \mathrm{b}/2] \tag{24}$$

$$\phi(\hat{x}, \hat{y}, \hat{w}) = V \cdot f(\hat{w}/\mathrm{g}), \quad \hat{x}\epsilon[-\mathrm{L}/2, \mathrm{L}/2], \quad \hat{y}\epsilon[-\mathrm{b}/2, \mathrm{b}/2] \tag{25}$$

where $\nabla^2 \equiv \frac{\partial}{\partial\hat{x}} + \frac{\partial}{\partial\hat{y}} + \frac{\partial}{\partial\hat{z}}$ stands for the Laplacian operator, $\hat{u}$ is the displacement of each point of the beam from $\hat{z} = 0$, V is the applied voltage, and the dimensionless function f is used to represent the fact that the voltage drop between the two plates may depend upon $\hat{u}$ [Pelesko and Triolo, 2001]. It is of special importance to remember that $\hat{u}$ should satisfy equation (12).

If nondimensional variables are introduced as in (13),

$$\psi = \frac{\phi}{V},\ w = \frac{\hat{w}}{\mathrm{g}},\ x = \frac{\hat{x}}{\mathrm{L}},\ y = \frac{\hat{y}}{\mathrm{b}},\ z = \frac{\hat{z}}{\mathrm{g}} \tag{26}$$

and substituted in equations (23)-(25), this yields

$$\epsilon^2\left(\frac{\partial^2\psi}{\partial x^2} + \mathrm{a}^2\frac{\partial^2\psi}{\partial y^2}\right) + \frac{\partial^2\psi}{\partial z^2} = 0, \tag{27}$$

$$\psi(x, y, 1) = 0, \quad x\epsilon[-1/2, 1/2], \quad y\epsilon[-1/2, 1/2] \tag{28}$$

$$\psi(x, y, w) = f(w), \quad x\epsilon[-1/2, 1/2], \quad y\epsilon[-1/2, 1/2] \tag{29}$$

where $\epsilon = \frac{\mathrm{g}}{\mathrm{L}}$ is an aspect ratio comparing the gap size to beam length and $\mathrm{a} = \frac{\mathrm{L}}{\mathrm{b}}$ is an aspect ratio of the beam design, comparing its length and width. Usually, in most applications the potential difference, V, is fixed and then $f(w) = 1$.

Using basic electrostatics equations, the *Potential Energy* stored between the capacitor plates is defined as [Jackson, 1962]

$$U_e(x, y, z) = \frac{\varepsilon V^2}{2}\int_v |\mathbf{E}|^2 \mathrm{d}v \tag{30}$$

where V is the potential difference between the capacitor plates, ε is the permeativity constant of the dielectric element between the plates (Free-space permeativity is $\varepsilon_0 = 8.854 \cdot 10^{-12} F/m$), $\int_v$ stands for the volume integral, $|\ |$ stands for a 2-norm of a vector and given that the *Electrostatic field* $\mathbf{E}$ is defined as

$$\mathbf{E} = -\nabla\psi \tag{31}$$

where ∇ is the gradient operator. From equation (30), the force generated by the electrostatic potential field in vacuum can be calculated as

$$F = -\nabla U_e = -\frac{\varepsilon_0 V^2}{2}|\nabla\psi|^2 \tag{32}$$

Consequently, the key problem to define the electrostatic force is solving the equation (27) for the electrostatic potential ψ.

Numerically, the potential can be calculated using finite elements [Pelesko and Triolo, 2001]. However, approximations can be done in order to develop the formulation.

The typical approximation is to consider that the plate width and longitude are considerably large against the gap between the plates, what implies that the force lines are basically parallel and the fringing fields are negligible. In this case, ϵ^2 in equation (27) is small, and the terms that are multiplied by this term can be ignored,

$$\frac{\partial^2\psi}{\partial z^2} = 0 \tag{33}$$

Then solving this equation for the potential ψ, it can be found that

$$\psi = \frac{f(w)(1-z)}{(1-w)} \tag{34}$$

and the differential force generated by this potential is

$$F(x,y) = -\frac{\varepsilon_0 V^2}{2\mathrm{g}^2(1-w)^2} \tag{35}$$

As can be observed, this approximation gives way to the expression of the force mostly used to calculate the electrostatic force between two parallel plates

$$F = -\frac{1}{2}\frac{\varepsilon_0 \mathrm{A}_c V^2}{\mathrm{g}^2(1-w)^2} \tag{36}$$

where A_c is the area of the capacitor plate. This formulation is only valid if the force contribution by the fringing fields that appear at the ends of the parallel plates can be assumed small compared to the total force.

This approximation is shown to be valid for the small aspect ratio devices. In [Pelesko and Triolo, 2001] and [Pelesko, 2001a] comparison between both approaches are presented and justifications of the validity of the approximation stated.

Another option to overcome the fringing fields is presented by [Nishiyama and Nakamura, 1990]. In this case, knowing that the charge distribution is not even and taking into account the effect of the fringing fields, a normalized capacitance C_n is derived that includes this effects. If in a parallel plate capacitor, the *capacitance* C is defined as the proportionality constant between the charge and the applied voltage

$$\mathrm{C} = \frac{\varepsilon \mathrm{bL}}{\mathrm{g}} \quad ; \quad Q = \mathrm{C}V \tag{37}$$

Then the *fringing-field corrected capacitance* $\tilde{\mathrm{C}}$ is defined as

$$\tilde{\mathrm{C}} = \mathrm{C}\mathrm{C}_n \tag{38}$$

where

$$\mathrm{C}_n = 1 + 4.246\vartheta, \qquad 0 \le \vartheta < 0.005 \tag{39}$$

$$\mathrm{C}_n = 1 + \sqrt{11.0872\vartheta^2 + 0.001097}, \quad 0.005 \le \vartheta < 0.05 \tag{40}$$

$$\mathrm{C}_n = 1 + 1.9861\vartheta^{0.8258}, \qquad 0.05 \le \vartheta \tag{41}$$

given that $\vartheta = \mathrm{g/b}$ is the aspect ratio of the gap against the width of the beam. The constants are derived applying regression analysis to numerically obtained data. The model has been validated to measured data [Nishiyama and Nakamura, 1990]. Other authors have obtained equivalent results with different fitting formulas.

Consequently, with this approximation, the force can be computed with

$$U = \frac{1}{2}\tilde{\mathrm{C}}V^2 = \frac{1}{2}\mathrm{C}_n\mathrm{C}V^2 = \frac{1}{2}\mathrm{C}_n\frac{\varepsilon \mathrm{bL}}{\mathrm{g}}V^2 \tag{42}$$

$$F = -\nabla U = \frac{1}{2}\mathrm{C}_n\frac{\varepsilon \mathrm{A}_c V^2}{\mathrm{g}^2(1-w)^2} \tag{43}$$

The derived expressions can be extended to non-uniform gap capacitors using sum of elementary capacitors [Najar et al., 2005].

3.3 Damping in MEMS

In Micro Electro Mechanical Systems, there are two basic sources of damping forces: structural damping and viscous damping (or aerodynamic damping).

The structural damping is generated by the molecular interaction in the material due to deformations. It happens in the moving parts and at the anchoring points [Duwel et al., 2003]. The main contribution has already been introduced in the mechanical model with the term including internal forces due to stretching. If the amplitude of oscillation of the beam is small, the values of these forces in materials like the polysilicon are negligible compared to the viscous damping effects.

The viscous damping effects appear due to the fluid that surrounds the MEMS device. The generated forces can be specially large if the fluid is air. For this reason, most devices are packaged in vacuum environments.

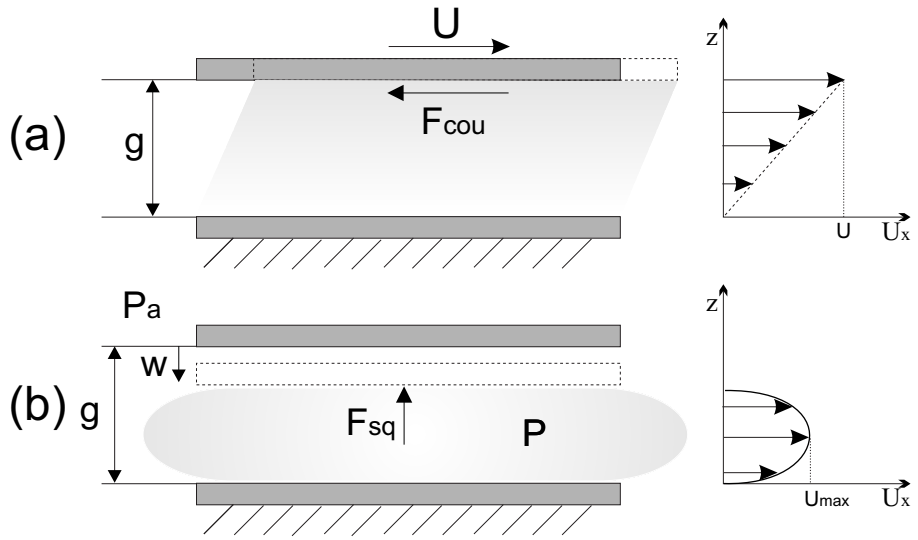

Figure 8: (a) Couette flow damping between two plates that move parallel one to the other and its velocity profile; (b) Squeeze film damping between two plates that move one against the other and its velocity profile.

Two different types of viscous damping can be usually identified in micromachined moving structures: *couette flow damping* and *squeeze film damping*.

To analyze the generated forces, one can turn to classical fluid mechanics and use the Navier-Stokes equations, which are composed of the continuity equation

$$\frac{\mathrm{D}\rho_m}{\mathrm{D}t} + \rho_m \nabla \mathbf{U} = 0 \tag{44}$$

and the motion equation

$$\rho_m \frac{\mathrm{D}\mathbf{U}}{\mathrm{D}t} = -\nabla P + \rho_m g + \eta \nabla^2 \mathbf{U} + \frac{\eta}{3} \nabla (\nabla \cdot \mathbf{U}) \tag{45}$$

where ρ_m is the mass-density of the fluid, η is the viscosity (assumed to be constant), g is the acceleration of gravity, P is the pressure of the fluid and $\mathbf{U}$ is the velocity of the fluid (bold symbol denotes that is a vector) [Pelesko and Bernstein, 2003].

In the *couette flow* case, the damping force appears between two plates that move parallel one to the other and are separated by a Newtonian fluid (Figure 8a) [Cho et al., 1994]. As the distance between the plates is considered constant, the working regime is under incompressible flow, meaning that the rate of change of density $\frac{\mathrm{D}\rho_m}{\mathrm{D}t}$ is negligible. Under this circumstances, the continuity equation (44) becomes

$$\nabla \mathbf{U} = 0 \tag{46}$$

and the Navier-Stokes equation of motion (45) reduces to

$$\rho_m \frac{\mathrm{D}\mathbf{U}}{\mathrm{D}t} = -\nabla P + \rho_m g + \eta \nabla^2 \mathbf{U} \tag{47}$$

for incompressible flow. The pressure and gravity terms can be combined introducing the position vector $\mathbf{r}$, and defining

$$P^* = P - \rho_m g \mathbf{r}$$

Using this definition, the Navier-Stokes equation reduces to the following steady-flow equation

$$\rho_m \frac{\mathrm{D}\mathbf{U}}{\mathrm{D}t} = \eta \nabla^2 \mathbf{U} - \nabla P^* \tag{48}$$

From Figure 8a, it can be seen that the flow becomes perfectly one-dimensional away from the edges. This aspect linked to condition (46) delimits that the velocity profile is composed of streamlines

$$\mathbf{U} = U_x(y)\mathbf{i}_x \tag{49}$$

and consequently,

$$\frac{\partial \mathbf{U}}{\partial t} = \mathbf{U} \cdot \nabla \mathbf{U} = \frac{D\mathbf{U}}{Dt} = 0 \tag{50}$$

Under these assumptions, and considering that no pressure gradient is generated by the moving plate, the Navier-Stokes equation reduces to

$$\frac{\partial^2 U_x}{\partial y^2} = 0 \tag{51}$$

giving a linear velocity profile as a solution.

If the fluid is liquid or gas, and the structures are relatively large (see [Veijola and Turowski, 2001] for correction in case of gas rarefication), one can apply the usual no-slip boundary condition, to the profile in Figure 8a. Then the velocity is

$$U_x = \frac{y}{\mathrm{g}} U \tag{52}$$

and the shear stress, using the Newtonian fluid condition, on the moving plate is

$$\tau = -\eta \frac{\partial U_x}{\partial y}|_{y=\mathrm{g}} = -\eta \frac{U}{\mathrm{g}} \mathbf{i}_x \tag{53}$$

Finally, the *couette damping force* of the whole structure can be calculated as

$$F_{cou} = -\eta \frac{A_{ov}}{\mathrm{g}} U = c_{cou} U \tag{54}$$

where the force is directly proportional to the velocity of the structure. A_{ov} is the area of overlapping between the structures.

However, in MEMS actuated with parallel plate capacitors, the main source of damping is the *Squeeze film force*. In this case, a moving plate move downwards and upwards from a fixed plate (Figure 8b). In this movement, when the plates approach each other the pressure in the trapped fluid increases, and the fluid is squeezed out through the edges of the plates. When the plates separate, a sucking drag is generated due to the fluid filling back the gap.

To solve this case, we must return to the Navier-Stokes equation (45), but this time we need the full compressible fluid equation. Consequently, to handle the analytical derivation, several assumptions must be done in our system:

- The aspect ratio is large, meaning that the gap is smaller than the plates extent.
- The motion is slow, meaning that the inertial term can be neglected in front of the viscous one, and the fluid works under Stokes flow.
- The pressure between the plates is homogeneous.
- The fluid flow at the edges of the plates follows a parabolic profile, defined by a Pousille-like equation (Figure 8b).
- The gas behaves under the ideal gas law.
- The system is isothermal.

Under these assumptions, the behavior of the fluid is governed by the Reynolds equation [Hamrock, 1994]

$$12\eta_{eff} \frac{\partial P d}{\partial t} = \nabla [d^3 P \nabla P] \tag{55}$$

where $P(x, y, t)$ is the pressure between the plates, $d(x, y, t)$ is the distance between the parallel plates, and η_{eff} is the corrected viscosity of the fluid, accounting for the rarefication effects due to low pressure [Veijola et al., 1995]

$$\eta_{eff} = \frac{\eta}{1 + 9.638 \mathrm{K}_n^{1.159}} \tag{56}$$

where $\mathrm{K}_n = \lambda / \mathrm{g}$ is the Knudsen number, which compares the mean free path of a fluid molecule (λ) against the gap distance. The constants are experimentally obtained. In a typical MEMS example, where λ is approximately 0.1 microns, the air is at atmospheric pressure and the gap is of 2 microns, the value of K_n would be 0.05. The mean free path is inversely proportional to fluid pressure.

Solution of equation (55) on P will lead to derivation of the *squeeze film forces*.

$$F_{sq} = (P - P_a) \cdot \mathrm{A}_c \tag{57}$$

where P_a is the static pressure force. As can be observed, the *squeeze forces* calculation is coupled to the mechanical deflection of the beam [Nayfeh and Younis, 2004].

To approximate the damping forces, one must linearize equation (55) assuming small amplitude motions. This way the gap distance and the pressure of the gap can be expressed as follows

$$d(x,y,t) = \mathrm{g} - w(x,y,t) \ ; \ P(x,y,t) = P_a + \bar{P}(x,y,t) \tag{58}$$

where w is the gap reduction and $\bar{P}$ the pressure variations from the static pressure. Substitution in (55) leads to

$$\frac{12\eta_{eff}}{P_a \mathrm{g}^3}\left(\mathrm{g}\frac{\partial \bar{P}}{\partial t} - P_a \frac{\partial w}{\partial t}\right) = \nabla^2 \bar{P} = \frac{\partial^2 \bar{P}}{\partial x^2} + \frac{\partial^2 \bar{P}}{\partial y^2} \tag{59}$$

From this equation [Nayfeh and Younis, 2004] has shown that numerical coupled perturbation methods can predict experimental damping forces accurately.

If we add the assumption that the capacitor plates are long and narrow (a beam), the equation can be much reduced due to the fact that the fluid movement is only in one direction (y-direction in our device)

$$\frac{\partial \bar{P}}{\partial t} = \frac{P_a \mathrm{g}^2}{12\eta_{eff}} \frac{\partial^2 \bar{P}}{\partial y^2} + \frac{P_a}{\mathrm{g}} \frac{\partial w}{\partial t} \tag{60}$$

From this equation, one can solve for $\bar{P}$, obtaining the following force on the capacitors [Senturia, 2001], using Laplace transform

$$F_{sq}(s) = \left[\frac{96\eta_{eff} L b^3}{\pi^4 \mathrm{g}^3} \sum_{nodd} \frac{1}{n^4} \frac{1}{1 + \frac{s}{\alpha_n}}\right] s z(s) \tag{61}$$

where

$$\alpha_n = \frac{\mathrm{g}^2 P_a n^2 \pi^2}{12\eta_{eff} b^2} \tag{62}$$

given that $z(s)$ is the input displacement. As we are assuming small amplitudes, the first term of the expansion is a good approximation of the force

$$F_{sq}(s) = \left[\frac{96\eta_{eff} L b^3}{\pi^4 \mathrm{g}^3} \frac{1}{1 + \frac{s}{\omega_c}}\right] s z(s) \tag{63}$$

From this derivation two important parameters arise, the *cut-off frequency*, ω_c

$$\omega_c = \frac{\pi^2 \mathrm{g}^2 P_a}{12\eta_{eff} b^2} \tag{64}$$

and the *squeeze number*, σ_d,

$$\sigma_d = \frac{\pi^2 \omega}{\omega_c} = \frac{12\eta_{eff} b^2}{\mathrm{g}^2 P_a} \omega \tag{65}$$

The squeeze number allow to analyze the behavior of the squeeze film damping forces. When the squeeze number decreases, due to low pressure or low frequencies of oscillation, the fluid force becomes a pure damping force. However, at high frequencies or high squeeze number, a spring force component appears and becomes dominant with the damping force still present. Example of the contributions of each force can be found in [Senturia, 2001]. Similar analysis and discussions are shown by [Andrews et al., 1993] and [Veijola et al., 1995] using the force decomposition derived in [Blech, 1983].

Consequently, squeeze film damping force can be reduced to

$$F_{sq} = c_{sq}(w, \sigma_d)\frac{\partial w}{\partial t} \tag{66}$$

with damping and spring effects depending on σ_d [Wang et al., 2004].

Finally, the fluid damping effects in the model are the combination of squeeze film and couette film damping, giving a final force

$$F_d = F_{sq} + F_{cou} = -\eta\frac{A_{ov}}{\mathrm{g}}U + (P - P_a)\cdot \mathrm{A}_c \tag{67}$$

that can be generalized as

$$F_d = (c_{sq} + c_{cou})\frac{\partial w}{\partial t} = \hat{c}_d\frac{\partial w}{\partial t} \tag{68}$$

3.4 Lumped system

The complete set of equations defining the behavior of the system can be obtained linking the different energies and non-conservative forces acting in the system.

The kinetic energy is defined in (7)

$$T = \frac{\rho \mathrm{bh}}{2}\int_0^{\mathrm{L}}\left(\frac{\partial \hat{w}}{\partial \hat{t}}\right)^2 \mathrm{d}\hat{x} \tag{69}$$

The potential energy is composed of mechanical (6),(8),(10) and electrostatic terms (30)

$$U = \frac{\mathrm{EI}}{2}\int_0^{\mathrm{L}}\left(\frac{\partial^2 \hat{w}}{\partial \hat{x}^2}\right)^2 \mathrm{d}\hat{x} + \frac{\hat{N}(\hat{t})}{2}\int_0^{\mathrm{L}}\left(\frac{\partial \hat{w}}{\partial \hat{x}}\right)^2 \mathrm{d}\hat{x} + \frac{\mathrm{bhE}}{8\mathrm{L}}\left[\int_0^{\mathrm{L}}\left(\frac{\partial \hat{w}}{\partial \hat{x}}\right)^2 \mathrm{d}\hat{x}\right]^2 + \frac{\varepsilon V^2}{2}\int_v |\nabla\psi|^2 \mathrm{d}v \tag{70}$$

The fluid damping is the only non-conservative force (67)

$$F_d = -\eta\frac{A_{ov}}{\mathrm{g}}U + (P - P_a)\cdot \mathrm{A}_c \tag{71}$$

Consequently, using Lagrange formulation and non-dimensional variables, the dynamics of the system is as follows:

$$\frac{\partial^4 w}{\partial x^4} + \frac{\partial^2 w}{\partial t^2} - \left[\alpha_1\Gamma(w, w) + N\right]\frac{\partial^2 w}{\partial x^2} = \gamma V^2|\nabla\psi|^2 - \frac{12\mathrm{L}^4}{\mathrm{E'\ h^3T}}\left[-\eta\frac{A_{ov}}{\mathrm{g}}U + (P - P_a)\cdot \mathrm{A}_c\right] \tag{72}$$

given that the electrostatic potential and the fluid pressure satisfy the following conditions

$$\epsilon^2\left(\frac{\partial^2\psi}{\partial x^2} + \mathrm{a}^2\frac{\partial^2\psi}{\partial y^2}\right) + \frac{\partial^2\psi}{\partial z^2} = 0 \tag{73}$$

$$12\eta_{eff}\frac{\partial Pd}{\partial t} = \nabla[d^3 P\nabla P] \tag{74}$$

Linking the different formulations previously derived , the dynamics of the system can be reduced to [Abdel-Rahman et al., 2003]:

$$\frac{\partial^2 w}{\partial t^2} + c\frac{\partial w}{\partial t} + \frac{\partial^4 w}{\partial x^4} - \left[\alpha_1\Gamma(w, w) + N\right]\frac{\partial^2 w}{\partial x^2} = \gamma V^2|\nabla\psi|^2 \tag{75}$$

$$w(0,t) = w(1,t) = 0, \quad w'(0,t) = w'(1,t) = 0$$

And the parameters appearing in equation (75) can be defined as follows

$$\begin{aligned} c &= \frac{\hat{c}_d \, \mathrm{L}^4}{\mathrm{E'} \, \mathrm{I} \, \mathrm{T}} \ , \quad N = \frac{\hat{N}\mathrm{L}^2}{\mathrm{E'I}} \\ \alpha_1 &= 6 \left(\frac{g}{h}\right)^2 \ , \quad \gamma = \frac{6\varepsilon_0 \mathrm{L}^4}{\mathrm{E'} \, \mathrm{h}^3 \mathrm{g}} \end{aligned} \tag{76}$$

Equation (75) translates to the following formulation once the electrostatic force is approximated

$$\frac{\partial^2 w}{\partial t^2} + c\frac{\partial w}{\partial t} + \frac{\partial^4 w}{\partial x^4} - \left[\alpha_1 \Gamma(w,w) + N\right] \frac{\partial^2 w}{\partial x^2} = \kappa \frac{V^2}{(1-w)^2} \tag{77}$$

where $\kappa = \frac{6\mathrm{C}_n \varepsilon_0 \mathrm{L}^4}{\mathrm{E'} \, \mathrm{h}^3 \mathrm{g}^3}$ using fringing fields correction.

4 Model solution

Once the model has been derived, one can analyze the behavior of the system.

In this section the different approaches to understand the system are presented and formulated. With each approach the advantages and problems are presented, as well as, the implications to the stability of the system.

4.1 Static solution

In the case of searching for the static solution of the system, the time-derivatives of the system must be set to zero. Under these premises, only potential energy terms remain in our system and the static solutions correspond to the equilibrium positions of the potential energy of the system, that is

$$\frac{dU}{d\hat{w}} = 0 \tag{78}$$

Consequently, the static deformation w_s of the beam, under the action of a electrostatic forcing V_p can be calculated from equation (75), if the time-derivatives are set to zero.

This way, the remaining terms are only position-dependant, and the partial differential equations disappear:

$$\frac{\mathrm{d}^4 w_s}{\mathrm{d}x^4} - \left[\alpha_1 \ \Gamma(w_s, w_s) + N\right] \frac{\mathrm{d}^2 w_s}{\mathrm{d}x^2} = \gamma V_p^2 |\nabla \psi|^2 \tag{79}$$

$$w_s = 0 \quad \textit{and} \quad \frac{\mathrm{d}w_s}{\mathrm{d}x} = 0 \quad \textit{at} \quad x = 0 \quad \textit{and} \quad x = 1 \tag{80}$$

Unfortunately, equation (79) do not generate a closed-form solution, due to its implicit nature. For this reason, numerical methods must be used to solve the problem.

A possibility is shooting methods combined with nonlinear boundary-value problem solution as in [Abdel-Rahman et al., 2003]. They apply the method to this model without fringing-fields correction ($\mathrm{C}_n = 1$).

$$\frac{\mathrm{d}^4 w_s}{\mathrm{d}x^4} - \left[\alpha_1 \ \Gamma(w_s, w_s) + N\right] \frac{\mathrm{d}^2 w_s}{\mathrm{d}x^2} = \kappa \frac{V^2}{(1-w)^2} \tag{81}$$

They show good agreement to experimental results, and argue that the inclusion of internal stretching is essential to predict real displacements. This approach allows to numerically calculate

the exact Static Pull-in Voltage using the same numerical method. Their analysis shows that neglecting the nonlinear effects leads to underestimating the stability limits of the system. The travel range taking into account the nonlinearities can be doubled.

Another option is to ignore the internal stretching, what reduces the model complexity, and use a method as the backward Euler algorithm to solve for the static displacement as in [Ijntema and Tilmans, 1992]:

$$\frac{\mathrm{d}^4 w_s}{\mathrm{d}x^4} - N\frac{\mathrm{d}^2 w_s}{\mathrm{d}x^2} = \kappa\frac{V^2}{(1-w)^2} \tag{82}$$

[Tilmans and Legtenberg, 1994] solved the same static problem using the Rayleigh-Ritz method assuming a combination of trial functions. They used this formulation to generate an analytical expression for the pull-in voltage, based on energy methods. Even with the needed approximations to solve the equations, the calculated values of the pull-in voltage were in good agreement with the results of experiments they conducted on resonators of various lengths. The system approximation generates good results while large amplitudes are not taken into account.

In [Zhou and Yang, 2003] numerical solutions are shown using the equation (82) and finite elements analysis. General numerical solutions using finite elements with reduced-order energy equations are presented in [Elata et al., 2003] using relaxation techniques. FEM solutions allow to handle the complete deformation of the device, without focusing on the maximum amplitude, but large computational time is needed.

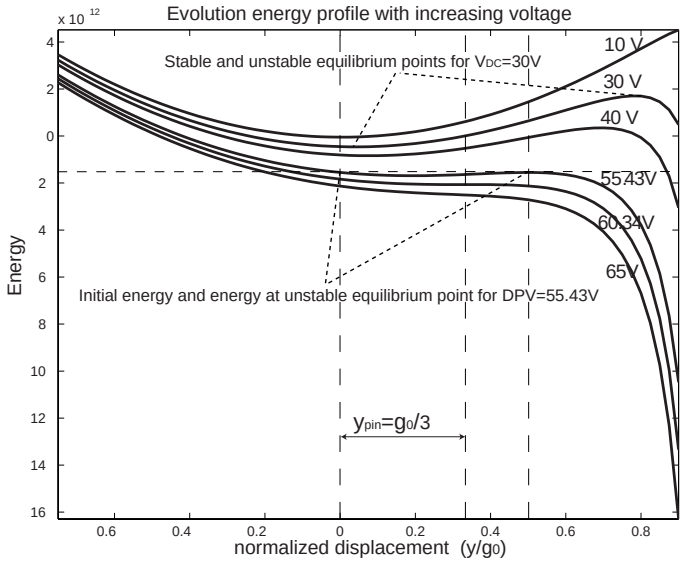

Figure 9: The Potential Energy levels of the a parallel-plate actuator system depend on the position relative to the gap. Energy of the system versus normalized displacement for different applied voltages are displayed for an example, including the *Static Pull-in Voltage* (60.34 V) and the *Dynamic Pull-in Voltage* (55.43 V). The stable equilibrium corresponds with the static displacement of the device.

Some elaborated solutions and behavior analysis are derived in [Bernstein et al., 2000] and [Pelesko, 2001a] directly form the differential equations. To arrive to the solutions, a simplified membrane model is used where the plate inertial and bending effects are neglected. However, numerical implicit formula solution is also needed to evaluate the static solution.

$$\frac{\mathrm{d}^2 u}{\mathrm{d}x^2} = \frac{\beta}{(1+u)^2} \tag{83}$$

This analysis allows to define stability conditions based on implicit eigenvalue equations.

Most authors work with the mass-spring-damper model, as in Figure 4. This model losses insight on the complete behavior of the system, but allow to analyze the system analytically, producing important information for the design process. The behavior of the beam can be approximated to that of a non-linear spring for a given deformation mode, as it has been shown in (19), and approximations can also be obtained for the electrostatic force and damping, giving way to the following formulation

$$M_{eff,i} \cdot \ddot{\hat{q}}_i + C_{eff,i} \cdot \dot{\hat{q}}_i + K_{eff,i} \cdot \hat{q}_i + K_{3,eff,i} \cdot \hat{q}_i^3 = F_e \tag{84}$$

In the static case, (84) simplifies to

$$K_{eff,i} \cdot \hat{q}_i + K_{3,eff,i} \cdot \hat{q}_i^3 = F_e \tag{85}$$

being a non-linear mass-spring equation. This model characterizes the beam stiffening due to large deformations, that reduces the effective travel range of the beam [Roessig, 1998].

However, in most cases small amplitude of oscillation is considered [Vinokur, 2002], [Gretillat et al., 1997] , allowing to use the linear formulation

$$K \cdot \hat{q}_i = -\frac{1}{2} \frac{\varepsilon_0 \mathrm{A}_c V^2}{\mathrm{g}^2 (1-w)^2} \tag{86}$$

With this model, the classical *Static Pull-in Voltage* (SPV) equation is obtained (Figure 9),

$$SPV = \sqrt{\frac{8}{27} \frac{K\, g_0^3}{\varepsilon_0\, A}}; y_{pin} = \frac{g_0}{3} \tag{87}$$

which indicates the maximum voltage that can be applied without getting snapping. Substitution of the voltage in the dynamics equation gives the maximum travel range in the static case, which is one-third of the initial gap [Senturia, 2001].

4.2 Dynamic solution

If we want to analyze the transient response of the microbeam when a variable voltage load $V(t)$ is applied, the complete evolution of the energy of the system has to be taken into account. To obtain solutions, the full set of equations (75) must be used.

Typical cases where the transient is of interest include micro-switches or mirror positioning, where the time response is of great interest. In this cases, the voltage is usually applied as a step-function or a ramp-function.

The use of numerical simulation to obtain the behavior of the system is mandatory if the complete set of equations is used. MEMS exhibit non-linearities even when the displacements are small, and the complete equations are needed to capture all the behavioral aspects.

The main dynamic nonlinear effects that will be detected on parallel-plate actuated MEMS are the following [Rand, 2003]:

- Spring stiffening: The effect appears due to large amplitudes of oscillation. The deformation of the beam cannot be considered linear anymore, and increases the beam resistance to deformation (19). The resulting non-linear equation corresponds to the Duffing equation (Figure 10a).

- Spring softening: The electrostatic force function (36) can be approximated using Taylor series. In that case, if only the first and second term are used, a negative spring term appears in the system equations. This fact is usually detected as a natural frequency reduction while increasing the voltage bias. This fact is used in some cases to adjust and trim the frequency of MEMS resonators [Painter and Shkel, 2003].

- Parametric excitation: The spring softening generated by the electrostatic force can derive to parametric excitation when an oscillatory force is used. In that case, the system behavior is governed by a Mathieu equation [Butikov, 2004]. Particular analysis can be carried out to analyze the parametric resonances and instabilities (Figure 10b).

- Hysteresis: Associated to the Duffing nonlinearity (Figure 10a), the system can derive to have bifurcation points that generate hysteresis regions in the behavior of the system [Gui et al., 1998], [Kaajakari et al., 2005].

- Chaos regions: Some works have analyzed the nonlinear behavior of parallel-plate actuated MEMS detecting existence of chaotic regions that could restrict the stable range of actuation of the devices [Liu et al., 2004] [Bienstman et al., 1998] [Wang et al., 1998].

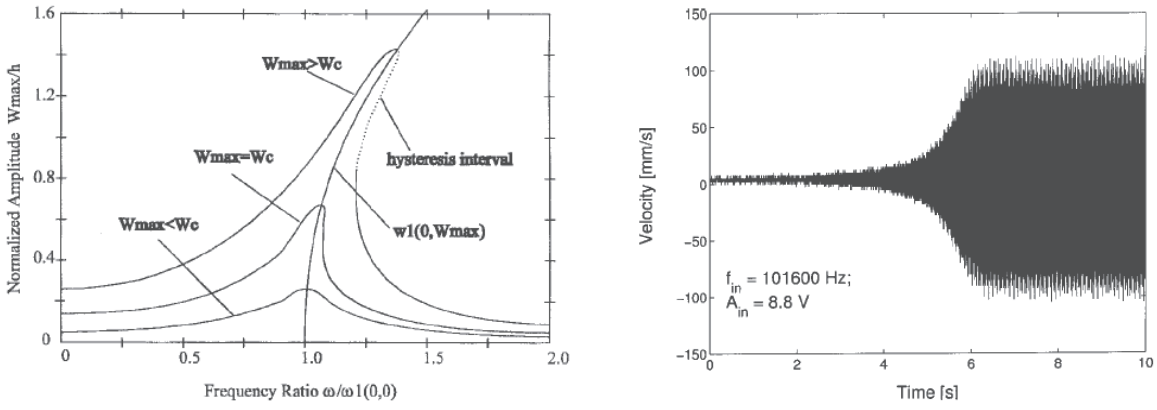

Figure 10: (a) Characteristic non-linear Duffing equation behavior of the frequency response of a parallel plate oscillator. As the amplitude increases, a hysteresis appears [Gui et al., 1998] ; (b) Characteristic profile of exponential growth during parametric excitation [Napoli et al., 2004]

A complete simulation of the system is presented in [Nayfeh and Younis, 2004], where the modeling and simulation under the effect of squeeze-film damping is analyzed. They use the compressible Reynolds equation coupled with the equation governing the plate deflection (72-74). The model accounts for the electrostatic forcing of the capacitor air-gap, the restoring force of the microplate and the applied in-plane loads. Perturbation methods are used to derive an analytical expression for the pressure distribution. This expression is then substituted into the plate equation, which is solved in turn using a finite-element method for the structural mode shapes, the pressure distributions, the natural frequencies and the quality factors.

Without taking the damping into account, some works analyze the electro-mechanical behavior. Analysis of the equations is carried out in [Xie et al., 2003] using a nonlinear modal analysis approach based on the invariant manifold method. Using Galerkin method, the nonlinear partial differential governing equation is decoupled into a set of nonlinear ordinary differential equations.

Then the invariant manifold method is used to obtain the associated nonlinear modal shapes, and modal motion governing equations. The model allows to examine the nonlinearities and the pull-in phenomena. Similar results using shooting methods combined with nonlinear boundary-value problem where presented in [Abdel-Rahman et al., 2002].

Using a simplified plate model (83), in [Flores et al., 2003] they obtain solutions of the system operated in viscous regime. This simplified mathematical model allows to study a parabolic equation of reaction-diffusion type. A central result of the paper is that when the applied voltage is beyond the critical voltage where steady-state solutions cease to exist, the solution touches down in finite time. Bounds on the touchdown time are computed and the structure of solutions near touchdown are investigated.

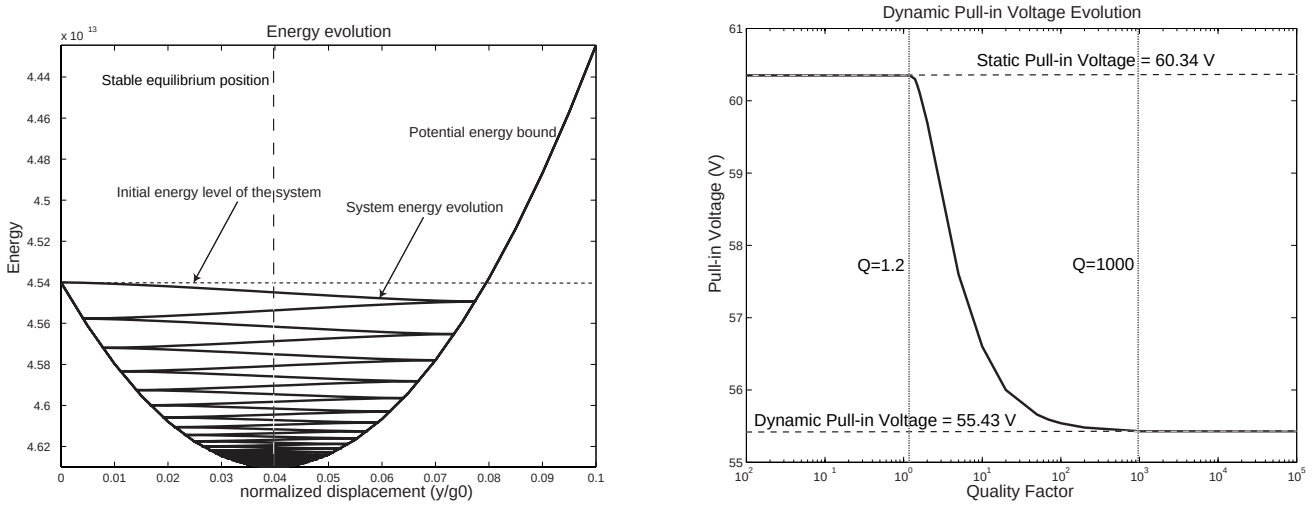

Figure 11: (a) Evolution of system's energy of an example when a 30 V step-function is applied. The Quality Factor in the example is 30. The initial energy corresponds to the potential energy (mechanical and electrostatic). When the motion begins, the potential energy is converted to kinetic energy and dissipation due to damping forces. The system's energy descends until reaching the stable equilibrium position; (b) Evolution of the pull-in voltage as a function of the Quality Factor in a example. For high-Q environments, the pull-in voltage corresponds to the *Dynamic Pull-in Voltage*. For low-Q environments, the pull-in voltage corresponds to the *Static Pull-in Voltage*. The calculation were done with a linear mass-spring-damper model.

The equations can be reduced to mass-spring-damper formulation as in [Krylov et al., 2005] and [Krylov and Maimon, 2004] in order to highlight leading dynamical phenomena through analysis of simplified expressions. They develop a model using the Galerkin procedure with normal modes as a basis. It accounts for the distributed nonlinear electrostatic forces, nonlinear squeezed film damping, and rotational inertia of a mass carried by the beam. Special attention is paid to the dynamics of the beam near instability points. The results generated by the model, and confirmed experimentally, show that nonlinear damping leads to shrinkage of the spatial region where stable motion is realizable. The model is useful to generate conclusions about the stability using the simplest model of a parametrically excited system described by Mathieu and Hills equations.

Energy methods are used in [Ligterink et al., 2005] to analyze the transient behavior between pull-in and release states. The concept of dynamic pull-in is addressed as well as hysteresis phenomena. No evolution analysis are performed.

Using mass-spring-damper models, linked to FEM analysis, interesting results can also be obtained. In [Han et al., 2005], model order reduction techniques are used to reduce the transient

analysis time. To do this, an open-source software performs model order reductions via the block Arnoldi algorithm directly to ANSYS finite element models.

On the other hand, direct analysis over the linear model can be useful in several applications (Figure 11a). The nonlinear behavior of the system with a simple mass-spring-damper model is analyzed in [ZHAO et al., 2005], [Castañer et al., 1999], [Minami et al., 1999]. In [Gupta and Senturia, 1997], they used the system analysis to predict pull-in times and derive the *Dynamic Pull-in Voltage* (DPV)

$$y_{uns} = \frac{g_0}{2} \; ; \; DPV = \sqrt{\frac{1}{4}\frac{K\, g_0^3}{\varepsilon_0\, A}} \tag{88}$$

which indicates the maximum voltage that can be applied as a step-function to the system without producing snapping in vacuum environment. A extended discussion on energy-dependence of the *Dynamic Pull-in Voltage* (Figure 11b) can be found in [Varghese et al., 1997] and [Fargas-Marques, 2001].

4.3 Oscillatory solution

In multiple applications in MEMS sensors and actuators, the system is oscillated at a fixed frequency. An alternating voltage is applied to the system to maintain the oscillation. The case of oscillatory load is, then, a sub-case of the dynamic solution.

To analyze the oscillatory case, the transient response is neglected and the efforts are concentrated on the stationary oscillation.

The microbeam deformation under an electrostatic excitation ($V(t) = Vp + v(t)$) is composed of a static component ($w_s(x)$) and a dynamic component ($u(x,t)$), due to the AC forcing voltage:

$$w(x,t) = w_s(x) + u(x,t) \tag{89}$$

To solve the oscillatory case, we substitute (89) in the dynamic equation of the system (75) and obtain

$$\begin{gathered}\frac{\partial^2(w_s(x)+u(x,t))}{\partial t^2} + c\frac{\partial(w_s(x)+u(x,t))}{\partial t} + \frac{\partial^4(w_s(x)+u(x,t))}{\partial x^4} \\ - \left[\alpha_1\Gamma((w_s(x)+u(x,t)),(w_s(x)+u(x,t))) + N\right]\frac{\partial^2(w_s(x)+u(x,t))}{\partial x^2} \\ = \gamma(V_p + v(t))^2|\nabla\psi|^2\end{gathered} \tag{90}$$

The equation can be simplified eliminating the expressions with null terms, and it turns to

$$\begin{gathered}\frac{\partial^2 u}{\partial t^2} + c\frac{\partial u}{\partial t} + \frac{\partial^4 w_s}{\partial x^4} + \frac{\partial^4 u}{\partial x^4} \\ - \left[\alpha_1(\Gamma(w_s,w_s) + 2\Gamma(w_s,u) + \Gamma(u,u)) + N\right]\left(\frac{\partial^2 w_s}{\partial x^2} + \frac{\partial^2 u}{\partial x^2}\right) \\ = \gamma(V_p + v(t))^2|\nabla\psi|^2\end{gathered} \tag{91}$$

Once in this point, to develop the equation further, a possibility is to approximate the electrostatic force, assuming no fringing fields, using equation (32). This way the oscillation is defined by

$$\begin{gathered}\frac{\partial^2 u}{\partial t^2} + c\frac{\partial u}{\partial t} + \frac{\partial^4 w_s}{\partial x^4} + \frac{\partial^4 u}{\partial x^4} \\ - \left[\alpha_1(\Gamma(w_s,w_s) + 2\Gamma(w_s,u) + \Gamma(u,u)) + N\right]\left(\frac{\partial^2 w_s}{\partial x^2} + \frac{\partial^2 u}{\partial x^2}\right) \\ = \alpha_2\frac{(V_p+v(t))^2}{(1-(w_s+u))^2}\end{gathered} \tag{92}$$

where now $\alpha_2 = \gamma/\mathrm{g}^2 = \frac{6\varepsilon_0 \mathrm{L}^4}{\mathrm{E'}\ \mathrm{h}^3\mathrm{g}^3}$.

The formulation can be much reduced if the electrostatic force is expanded in Taylor series around the equilibrium position

$$\begin{aligned}
&\tfrac{\partial^2 u}{\partial t^2} + c\tfrac{\partial u}{\partial t} + \tfrac{\partial^4 w_s}{\partial x^4} + \tfrac{\partial^4 u}{\partial x^4} \\
&- \left[\alpha_1(\Gamma(w_s,w_s) + 2\Gamma(w_s,u) + \Gamma(u,u)) + N\right](\tfrac{\partial^2 w_s}{\partial x^2} + \tfrac{\partial^2 u}{\partial x^2}) \\
&= \alpha_2(V_p^2 + 2V_p v(t) + v(t)^2)\left(\tfrac{1}{\beta^2} + \tfrac{2}{\beta^3}u + \tfrac{3}{\beta^4}u^2 + \tfrac{4}{\beta^5}u^3 + O(u^4)\right)
\end{aligned} \tag{93}$$

and then, rearranging terms, the static solution (79) can be eliminated and only the oscillating solution is conserved, simplifying the equation to

$$\begin{aligned}
&\tfrac{\partial^2 u}{\partial t^2} + c\tfrac{\partial u}{\partial t} + \tfrac{\partial^4 u}{\partial x^4} \\
&-\alpha_1\left[2\Gamma(w_s,u) + \Gamma(u,u)\right]\tfrac{\partial^2 w_s}{\partial x^2} \\
&- \left[\alpha_1(\Gamma(w_s,w_s) + 2\Gamma(w_s,u) + \Gamma(u,u)) + N\right]\tfrac{\partial^2 u}{\partial x^2} \\
&= \alpha_2 V_p^2\left(\tfrac{2}{\beta^3}u + \tfrac{3}{\beta^4}u^2 + \tfrac{4}{\beta^5}u^3 + O(u^4)\right) \\
&+2\alpha_2 V_p v(t)\left(\tfrac{1}{\beta^2} + \tfrac{2}{\beta^3}u + \tfrac{3}{\beta^4}u^2 + \tfrac{4}{\beta^5}u^3 + O(u^4)\right) \\
&+\alpha_2 v(t)^2\left(\tfrac{1}{\beta^2} + \tfrac{2}{\beta^3}u + \tfrac{3}{\beta^4}u^2 + \tfrac{4}{\beta^5}u^3 + O(u^4)\right)
\end{aligned} \tag{94}$$

Depending on the driving voltages and the accepted error, the final equation can be selected. However, numerical simulation will be needed to obtain evolution results.

Complete simulations based on the theoretical framework exist in the literature. In [Abdel-Rahman et al., 2003], shooting methods combined with nonlinear boundary-value problem are used to solve the existing eigenvalue problem. The vibrations around the deflected position of the microbeam are solved numerically for various parameters to obtain the natural frequencies and mode shapes. The results are compared with experimental results available in the literature with good agreement. In [Nayfeh and Younis, 2004], perturbation methods are used to obtain the mode shapes and frequencies including the coupled effects of the squeeze-film damping that were just approximated in the previous analysis.

Following the same study, in [Younis et al., 2004] they present a methodology to simulate the transient and steady-state dynamics of microbeams undergoing small or large motions actuated by combined DC and AC loads. They use the model to produce results showing the effect of varying the DC bias, the damping, and the AC excitation amplitude on the frequency-response curves. In their analysis they detect the existence of dynamic effects that can produce pull-in with electric loads much lower than that predicted based on static analysis.

In [Ijntema and Tilmans, 1992], the dynamic behavior is modeled using energy methods to obtain a spring-mass-damper model. The fundamental frequency is approximated using Rayleigh's energy method where the microbeam motion is linearized around the deflected shape obtained as a solution of the static problem. The work is extended in [Tilmans and Legtenberg, 1994] where the fundamental natural frequency obtained from Rayleigh's energy method is compared to the experimentally obtained fundamental natural frequency. They found out that the results obtained from the expression were only valid for small dc polarization voltages away from the pull-in voltage. Their method takes into account the axial load and large amplitude effects.

The mass-spring-damper formulation obtained via Galerkin procedure in [Krylov et al., 2005] allows to study the parametric resonance behavior of the system. They show that parametric stabilization can be obtained. The model summarizes the main nonlinearities for a given frequency. Similar analysis are carried out with a parametric model in [Napoli et al., 2004] They show that the underlying linearized dynamics of the system are those of a periodic system described by a Mathieu

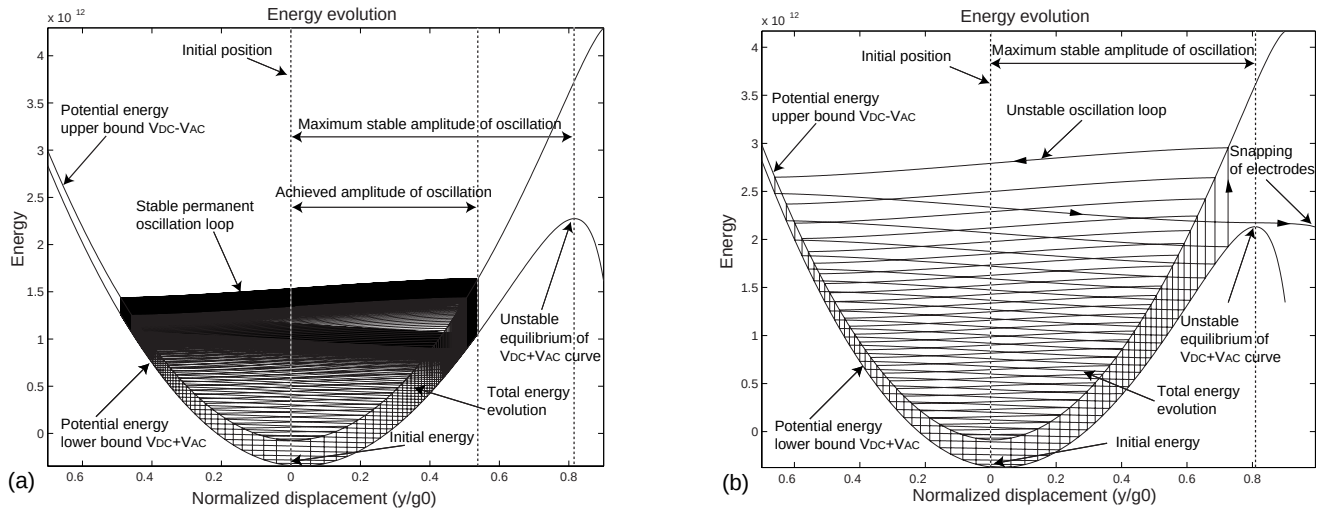

Figure 12: The potential energy curves bound the system oscillation. In (a) a stable oscillation is obtained for the example system with 19 V_{DC} bias voltage and a 7 V_{AC} amplitude while in (b) the oscillation is unstable with 20 V_{DC} and 7 V_{AC}. Beginning from the static initial position, the amplitude of oscillation increases until it reaches the unstable equilibrium point at $V_{DC} + V_{AC}$, resulting in snapping.

equation. Experimental results confirm the validity of the model, and in particular, illustrate that parametric resonance phenomena occur in capacitively actuated micro-cantilevers.

Finite element approaches are also valid to obtain the behavior of the system [Gretillat et al., 1997]. However computation times can be quite demanding in the case of non-linear coupling.

In [Hung, 1997], it is shown that a way of solving the simulation of the system is rewriting the solution as a sum of orthogonal basis functions, that correspond to the oscillation modes. They show the feasibility using an initial model with internal tension and damping. The obtained low-order models are quicker for numerical modeling.

Multiple authors have modeled a microbeam under electrostatic actuation as a single-degree-of-freedom spring-mass-damper system. The model assumes a linear spring, thus neglects midplane stretching effects. They use this model to generate an analytical expression for the fundamental natural frequency as a function of the dc polarization voltage. Both this expression and the experiments they carry on a resonator show that increasing the dc polarization voltage decreases the fundamental natural frequency [Vinokur, 2002], [Seeger, 1997], [Sung et al., 2003].

Using a spring-mass-damper model and energy methods, the AC Pull-in Voltage is presented and analyzed in [Fargas-Marques, 2001] as the combination of V_{DC} and V_{AC} that can lead the system to snapping (Figure 12). Numerical and experimental results are presented to validate the concept. Similar results are presented in [Seeger and Boser, 2002] for double-sided actuated oscillators near the mechanical resonant frequency and amplitudes comparable to the actuator gap. They show that at resonance, the structure can move beyond the well-known pull-in-limit but is instead limited to 56% of the gap by resonant pull-in. Above the resonant frequency, the structure is not limited by pull-in and can theoretically oscillate across the entire gap.

5 Final Conclusions

Correct modeling of parallel-plate electrostatic actuation of MEMS is an important step to design better MEMS devices. It has been shown that different approaches can be taken to try to capture the behavior of the devices, but lots of issues are yet to be solved.

This work has tried to compile the main approaches in the literature in order to analyze the advantages of each one. The main conclusion achieved is that depending on the goal while designing MEMS actuators, the complexity of the model has to be evaluated. Complete models involved time-consuming calculations while reduced models imply reduced accuracy.

Table 2 shows a summarized classification of the different approaches in the literature and the addressed phenomena.

Future work should address an uniformed way of analyzing Pull-in given a generalized and its implications on control of oscillatory MEMS.

	Differential Eq.	Numerical Sol.	Simple Model	Parametric excitation	Modal/Energy Analysis
Static Solution	[Abdel-Rahman et al., 2002] [Pelesko and Triolo, 2000] [Pelesko, 2001b] [Flores et al., 2003]	[Aluru and White, 1999] [Ananthasuresh et al., 1996] [Elata et al., 2003]	[Saucedo-Flores et al., 2004] [Chu et al., 1996] [Ijntema and Tilmans, 1992]		[Tilmans and Legtenberg, 1994] [Ijntema and Tilmans, 1992]
Dynamic Solution	[Abdel-Rahman et al., 2002] [Flores et al., 2003] [Younis et al., 2004] [Abdel-Rahman et al., 2003] [Xie et al., 2003]	[Ananthasuresh et al., 1996]	[Saucedo-Flores et al., 2004] [Ijntema and Tilmans, 1992] [Castañer and Senturia, 1999] [YEH et al., 2001] [Gupta and Senturia, 1997]	[Butikov, 2004] [Napoli et al., 2003b] [Napoli et al., 2003a]	[Tilmans and Legtenberg, 1994] [Ijntema and Tilmans, 1992] [Yang et al., 1997] [Roessig, 1998]
Static Pull-in	[Abdel-Rahman et al., 2002] [Pelesko and Triolo, 2000] [Pelesko, 2001b] [Flores et al., 2003]	[Ananthasuresh et al., 1996] [Elata et al., 2003]	[Saucedo-Flores et al., 2004] [Chu et al., 1996] [Rocha et al., 2004]		[Tilmans and Legtenberg, 1994] [Huang et al., 2003]
Dynamic Pull-in	[Abdel-Rahman et al., 2002] [Flores et al., 2003] [Younis et al., 2004]	[Ananthasuresh et al., 1996]	[Gupta and Senturia, 1997] [Castañer and Senturia, 1999] [Rocha et al., 2004]		[Tilmans and Legtenberg, 1994]
K softening	[Younis and Nayfeh, 2003]	[Ananthasuresh et al., 1996]			[Tilmans and Legtenberg, 1994] [Roessig, 1998]
AC actuation	[Abdel-Rahman et al., 2002] [Younis and Nayfeh, 2003] [Krylov and Maimon, 2004]		[Seeger and Boser, 2002]		[Tilmans and Legtenberg, 1994] [Roessig, 1998]
Large amplitude	[Abdel-Rahman et al., 2002] [Younis and Nayfeh, 2003]			[Napoli et al., 2003b] [Zhang et al., 2002]	[Tilmans and Legtenberg, 1994] [Roessig, 1998]
Tension sensitivity	[Abdel-Rahman et al., 2002] [Younis and Nayfeh, 2003]				[Tilmans and Legtenberg, 1994] [Roessig, 1998]
Control	[Pelesko and Triolo, 2000]		[Castañer and Senturia, 1999] [YEH et al., 2001] [Sung et al., 2000]	[Napoli et al., 2003a]	
Stability	[Pelesko and Triolo, 2000] [Flores et al., 2003] [Younis et al., 2004]		[Pelesko and Bernstein, 2003]	[Butikov, 2004] [Napoli et al., 2003a]	[Ijntema and Tilmans, 1992]
Damping		[Yang and Senturia, 1996]	[Chu et al., 1996] [Gupta and Senturia, 1997]	[Zhang et al., 2002]	[Yang et al., 1997]
Comparison to reality	[Abdel-Rahman et al., 2002]	[Ananthasuresh et al., 1996]	[Chu et al., 1996]	[Napoli et al., 2003b] [Napoli et al., 2003a] [Zhang et al., 2002]	[Tilmans and Legtenberg, 1994] [Huang et al., 2003]
Model comparison		[Aluru and White, 1999]			[Ijntema and Tilmans, 1992] [Huang et al., 2003]

Table 2: Comparison of the different analysis approaches in the literature

References

[Abdel-Rahman et al., 2003] Abdel-Rahman, E. M., Nayfeh, A. H., and Younis, M. I. (2003). Dynamics of an electrically actuated resonant microsensor. In *International Conference on MEMS, NANO and Smart Systems*.

[Abdel-Rahman et al., 2002] Abdel-Rahman, E. M., Younis, M. I., and Nayfeh, A. H. (2002). Characterization of the mechanical behavior of an electrically actuated microbeam. *Micromechanics and Microengineering*.

[Aluru and White, 1999] Aluru, N. R. and White, J. (1999). A multilevel newton method for mixed-energy domain simulation of mems. *Journal of Microelectromechanical Systems*.

[Ananthasuresh et al., 1996] Ananthasuresh, G. K., Gupta, R. K., and Senturia, S. D. (1996). An approach to macromodeling of mems for nonlinear dynamic simulation. In *International Mechanical Engineering Congress and Exposition*. ASME.

[Andrews et al., 1993] Andrews, M., Harris, I., and Turner, G. (1993). A comparison of squeeze-film theory with measurements on a microstructure. *Sensors and Actuators A*.

[Attia et al., 1998] Attia, P., Bontry, M., Bossehoeuf, A., and Hesto, P. (1998). Fabrication and characterization of electrostatically driven silicon microbeams. *J. Microelectronics*, 29:pp. 641–644.

[Bernstein et al., 2000] Bernstein, D., Guidotti, P., and Pelesko, J. (2000). Mathematical analysis of an electrostatically actuated mems devices. *MSM*.

[Bienstman et al., 1998] Bienstman, J., Puers, R., and Vandewalle, J. (1998). Periodic and chaotic behaviour of the autonomous impact resonator. *IEEE*.

[Blanc et al., 1996] Blanc, N., Brugger, J., de Rooji, N., and Durig, U. (1996). Scanning force microscopy in the dynamic mode using microfabricated capacitive sensors. *J. Vac. Sci. Technol*, 14(2):pp.901–905.

[Blech, 1983] Blech, J. (1983). On isothermal squeeze films. *Journal of Lubrication Technology*, page 615.

[Brosnihan et al., 1995] Brosnihan, T. J., Pisano, A., and Howe, R. (1995). Surface-micromachined angular accelerometer with force feedback. In *ASME Dynamic Systems and Control Division*. ASME.

[Burns et al., 1995] Burns, D., Zook, J., Horning, R., Herb, W., and Guckel, H. (1995). Sealed-cavity resonant microbeam pressure sensor. *Sensors and Actuators A*, 48(3):179–186.

[Burstein, 1995] Burstein, A. Kaiser, W. (1995). Mixed analog-digital highly-sensitive sensor interface circuit for low-cost microsensors. *Solid-State Sensors and Actuators, 1995 and Eurosensors IX. Transducers '95. The 8th International Conference on*.

[Butikov, 2004] Butikov, E. I. (2004). Parametric excitation of a linear oscillator. *European Journal of Physics*.

[Castañer et al., 1999] Castañer, L., Rodriguez, A., Pons, J., and Senturia, S. D. (1999). Pull-in time-energy product of electrostatic actuators: comparison of experiments with simulation. *Sensors and Actuators A*, 83(1-3):263–269.

[Castañer and Senturia, 1999] Castañer, L. M. and Senturia, S. D. (1999). Speed-energy optimization of electrostatic actuators based on pull-in. *IEEE Journal of Micromechanical Systems*, 8(3):290–298.

[Cho et al., 1994] Cho, Y.-H., Kwak, B. M., Pisano, A. P., and Howe, R. T. (1994). Slide film damping in laterally driven microstructures. *Sensors and Actuators A: Physical*.

[Chu et al., 1996] Chu, P. B., Nelson, P. R., Tachiki, M. L., and Pister, K. S. (1996). Dynamics of polysilicon parallel-plate electrostatic actuators. *Sensors and Actuators A*, 52:216–220.

[Chui et al., 1998] Chui, B., Kenny, T., Mamin, H., Terris, B., and Rugar, D. (1998). Independent detection of vertical and lateral forces wilh a sidewall-implanted dual-axis piezoresistive cantilever. *Appl. Phys. Lett.*, 72(11):pp.1388– 1390.

[Dauwalter and Ha, 2004] Dauwalter, C. and Ha, J. (2004). A high performance magnetically suspended mems spinning wheel gyro. *Position Location and Navigation Symposium, 2004. PLANS*.

[Duwel et al., 2003] Duwel, A., Gorman, J., Weinstein, M., Borenstein, J., and Ward, P. (2003). Experimental study of thermoelastic damping in mems gyros. *Sensors and Actuators A*.

[Elata et al., 2003] Elata, D., Bochobza-Degani, O., Feldman, S., and Nemirovsky, Y. (2003). Secondary dof and their effect on the instability of electrostatic mems devices. *Micro Electro Mechanical Systems, 2003. MEMS-03 Kyoto. IEEE The Sixteenth Annual International Conference on*.

[Fargas-Marques, 2001] Fargas-Marques, A. (2001). Stable electrostatic actuation of mems double-ended tuning fork oscillators. Master's thesis, University of California, Irvine. Advisor: Dr. Shkel.

[Flores et al., 2003] Flores, G., Mercado, G., and Pelesko, J. (2003). Dynamics and touchdown in electrostatic mems. In *MEMS, NANO and Smart Systems, 2003. Proceedings. International Conference on*, pages Pages: 182– 187.

[Gaucher et al., 1998] Gaucher, P., Eichner, D., Hector, J., and von Munch, W. (1998). Piezoelectric bimorph cantilever for actuationf and sensing applications. *J. Phys. IV France*, 8:pp. 235–238.

[Gretillat et al., 1997] Gretillat, M.-A., Yang, Y.-J., Hung, E., Rabinovich, V., Ananthasuresh, G., De Rooij, N., and Senturia, S. (1997). Nonlinear electromechanical behaviour of an electrostatic microrelay. *Solid State Sensors and Actuators, 1997. TRANSDUCERS '97*.

[Gui et al., 1998] Gui, C., Legtenberg, R., Tilmans, H. A. C., Fluitman, J. H. J., , and Elwenspoek, M. (1998). Nonlinearity and hysteresis of resonant strain gauges. *Microelectromechanical Systems*, 7.

[Gupta and Senturia, 1997] Gupta, R. K. and Senturia, S. (1997). Pull-in time dynamics as a measure of absolute pressure. In *The Tenth Annual International Workshop on Micro Electro Mechanical Systems*, pages 290–294.

[Hamrock, 1994] Hamrock, B. (1994). *Fundamentals of fluid film lubrication*. McGraw Hill.

[Han et al., 2005] Han, J. S., Rudnyi, E. B., and Korvink, J. G. (2005). Efficient optimization of transient dynamic problems in mems devices using model order reduction. *Journal of Micromechanics and Microengineering*.

[Huang et al., 2003] Huang, J.-M., Liu, A., Lu, C., and Ahn, J. (2003). Mechanical characterization of micromachined capacitive switches: design consideration and experimental verification. *Sensors and Actuators A*.

[Huang and Lee, 2000] Huang, Q. and Lee, N. (2000). A simple approach to characterizing the driving force of polysilicon laterally driven thermal microactuators. *Sensors and Actuators*, 80:pp. 267–272.

[Hung, 1997] Hung, E.S. Yao-Joe Yang Senturia, S. (1997). Low-order models for fast dynamical simulation of mems microstructures. *Solid State Sensors and Actuators, 1997. TRANSDUCERS '97*.

[Ijntema and Tilmans, 1992] Ijntema, D. J. and Tilmans, H. A. C. (1992). Static and dynamic aspects of an air-gap capacitor. *Sensors and Actuators A: Physical*.

[Itoh et al., 1996] Itoh, T., Ohashi, T., and Suga, T. (1996). Piezoelectric cantilever array for multiprobe scanning force microscopy. In *Proc. of the IX Int. Workshop on MEMS*, pages 451–455, San Diego.

[Jackson, 1962] Jackson, J. D. (1962). *Classical electrodynamics*. John Wiley & Sons.

[Jonsmann et al., 1999] Jonsmann, J., Sigmund, O., and Bouwstra, S. (1999). Compliant electro-thermal microactuators. *IEEE*.

[Juneau et al., 2003] Juneau, T., Unterkofler, K., Seliverstov, T., Zhang, S., and Judy, M. (2003). Dual-axis optical mirror positioning using a nonlinear closed-loop controller. *TRANSDUCERS, Solid-State Sensors, Actuators and Microsystems, 12th International Conference on,*.

[Juneau, 1997] Juneau, T. N. (1997). *Micromachined Dual Input Axis Rate Gyroscope*. PhD thesis, U.C. Berkeley.

[Kaajakari et al., 2005] Kaajakari, V., Mattila, T., Lipsanen, A., and Oja, A. (2005). Nonlinear mechanical effects in silicon longitudinal mode beam resonators. *Sensors and Actuators A: Physical*, 120(1):64–70.

[Kovacs, 1998] Kovacs, G. (1998). *Micromachined Transducers Sourcebook*. McGraw-Hill.

[Kranz et al., 2003] Kranz, M., Burgett, S., Hudson, T., Buncick, M., Ruffin, P., Ashley, P., and McKee, J. (2003). A wide dynamic range silicon-on-insulator mems gyroscope with digital force feedback. *TRANSDUCERS, Solid-State Sensors, Actuators and Microsystems, 12th International Conference on,*.

[Krylov et al., 2005] Krylov, S., Harari, I., and Cohen, Y. (2005). Stabilization of electrostatically actuated microstructures using parametric excitation. *Journal of Micromechanics and Microengineering*, 15:11881204.

[Krylov and Maimon, 2004] Krylov, S. and Maimon, R. (2004). Pull-in dynamics of an elastic beam actuated by continuously distributed electrostatic force. *Transactions of the ASME - L - Journal of Vibration and Acoustics*, 126(3).

[Kuehnel, 1995] Kuehnel, W. (1995). Modelling of the mechanical behaviour of a differential capacitor acceleration sensor. *Sensors and Actuators A: Physical*.

[Lee, 1997] Lee, M. (1997). Merged technology on mems. In *Electron Devices Meeting, . Proceedings*.

[Lethbridge et al., 1993] Lethbridge, J., Cheshmehdoost, A., C.M.France, and Jones, B. (1993). An optical-fibre hybrid pressure transducer employing a mechanical resonator. *Sensors and Actuators A*, 37-38:480–483.

[Ligterink et al., 2005] Ligterink, N., Patrascu, M., Breedveld, P., and Stramigioli, S. (2005). An energy-based electroelastic beam model for mems applications. *Sensors and Actuators A*, 121.

[Liu et al., 2004] Liu, S., Davidson, A., and Lin, Q. (2004). Simulation studies on nonlinear dynamics and chaos in a mems cantilever control system. *Micromechanics and Microengineering*.

[M Hashimoto and Esashi, 1995] M Hashimoto, C Cabuz, K. M. and Esashi, M. (1995). Silicon resonant angular rate sensor using electromagnetic excitation and capacitive detection. *Micromechanics and Microengineering*.

[Minami et al., 1999] Minami, K., Matsunaga, T., and Esashi, M. (1999). Simple modeling and simulation of the squeeze film effect and transient response of the mems device. In *Micro Electro Mechanical Systems, 1999. MEMS '99*.

[Minne et al., 1995] Minne, S., Manalis, S., and Quate, C. (1995). Parallel atomic force microscopy using cantilevers with integrated piezoresistive sensors and integrated piezoelectric actuators. *Appl. Phys. Lett.*, 67(26):pp. 3918–3920.

[Najar et al., 2005] Najar, F., Choura, S., El-Borgi, S., Abdel-Rahman, E. M., and Nayfeh, A. H. (2005). Modeling and design of variable-geometry electrostatic microactuators. *Journal of Micromechanics and Microengineering*.

[Napoli et al., 2003a] Napoli, M., Bamieh, B., and Turner, K. (2003a). Mathematical modeling, experimental validation and observer design for a capacitively actuated microcantilever. In *American Control Conference, 2003. Proceedings of the*.

[Napoli et al., 2004] Napoli, M., Bamieh, B., and Turner, K. (2004). A capacitive microcantilever: Modelling, validation, and estimation using current measurements. *Journal of Dynamic Systems, Measurement, and Control*, 126(2):319–326.

[Napoli et al., 2003b] Napoli, M., Turner, W. Z., and K. Bamieh, B. (2003b). Dynamics of mechanically and electrostatically coupled microcantilevers. *TRANSDUCERS, Solid-State Sensors, Actuators and Microsystems, 12th International Conference on,.*

[Nathanson et al., 1967] Nathanson, H., Newell, W., Wickstrom, R., and J.R. Davis, J. (1967). The resonant gate transistor. *IEEE Transactions on Electronics devices*.

[Nayfeh and Younis, 2004] Nayfeh, A. H. and Younis, M. I. (2004). A new approach to the modeling and simulation of flexible microstructures under the effect of squeeze-film damping. *Journal of Micromechanics and Microengineering*.

[Newell, 1968] Newell, W. (1968). Miniaturization of tuning forks. *Science*, 161(3848):1320–1326.

[Niarchos, 2003] Niarchos, D. (2003). Magnetic mems: key issues and some applications. *Sensors and Actuators A*.

[Nishiyama and Nakamura, 1990] Nishiyama, H. and Nakamura, M. (1990). Capacitance of a strip capacitor. *Components, Hybrids, and Manufacturing Technology, IEEE Transactions on*.

[Oz and Fedder, 2003] Oz, A. and Fedder, G. (2003). Rf cmos-mems capacitor having large tuning range. *TRANSDUCERS, Solid-State Sensors, Actuators and Microsystems, 12th International Conference on,*.

[Pai and Tien, 2000] Pai, M. and Tien, N. C. (2000). Low voltage electrothermal vibromotor for silicon optical bench applications. *Sensors and Actuators*.

[Painter and Shkel, 2003] Painter, C. C. and Shkel, A. M. (2003). Active structural error suppression in mems vibratory rate integrating gyroscopes. *IEEE SENSORS JOURNAL*.

[Pelesko, 2001a] Pelesko, J. (2001a). Electrostatic field aproximations and implications for mems devices. *Proceedings of ESA*.

[Pelesko, 2001b] Pelesko, J. (2001b). Multiple solutions in electrostatic mems. *Proceedings of Modeling and Simulation of Microsystems 2001, Hilton Head*.

[Pelesko and Triolo, 2000] Pelesko, J. and Triolo, A. (2000). Nonlocal problems in mems device control. In *Technical Proceedings of the 2000 International Conference on Modeling and Simulation of Microsystems*.

[Pelesko and Triolo, 2001] Pelesko, J. and Triolo, A. (2001). Nonlocal problems in mems device control. *Journal of Engineering Mathematics*, 41.

[Pelesko and Bernstein, 2003] Pelesko, J. A. and Bernstein, D. H. (2003). *Modeling MEMS and NEMS*. Chapman & Hall/CRC. ISBN: 1-58488-306-5.

[Rand, 2003] Rand, R. H. (2003). *Lecture Notes on Nonlinear Vibrations, version 45*. Available online at http://www.tam.cornell.edu/randdocs/.

[Rao and Raju, 2003] Rao, G. and Raju, K. (2003). Large amplitude free vibrations of beams - an energy approach. *ZAMM - Journal of Applied Mathematics and Mechanics*, 83(7):493 – 498.

[Rao, 1990] Rao, S. (1990). *Mechanical Vibrations*. Addison-Wesley, 2nd edition.

[Robert et al., 2003] Robert, P., Saias, D., Billard, C., Boret, S., Sillon, N., Maeder-Pachurka, C., Charvet, P., Bouche, G., Ancey, P., and Berruyer, P. (2003). Integrated rf-mems switch based on a combination of thermal and electrostatic actuation. *TRANSDUCERS, Solid-State Sensors, Actuators and Microsystems, 12th International Conference on,*.

[Rocha et al., 2004] Rocha, L., Cretu, E., and Wolffenbuttel, R. (2004). Pull-in dynamics: analysis and modeling of the transitional regime. In *Micro Electro Mechanical Systems,*.

[Roessig, 1995] Roessig, T. A. W. (1995). Surface micromachined resonant force transducers. Master's thesis, U.C. Berkeley.

[Roessig, 1998] Roessig, T. A. W. (1998). *Integrated MEMS Tuning Fork Oscillators for Sensor Applications*. PhD thesis, U.C. Berkeley.

[Sane and Yazdi, 2003] Sane, H. and Yazdi, N.and Mastrangelo, C. (2003). Application of sliding mode control to electrostatically actuated two-axis gimbaled micromirrors. In *American Control Conference, 2003. Proceedings of the 2003*.

[Saucedo-Flores et al., 2004] Saucedo-Flores, E., Ruelas, R., Flores, M., Ying, C., and Jung-chih., C. (2004). Dynamic behavior modeling of mems parallel plate capacitors. *PLANS 2004. Position Location and Navigation Symposium (IEEE Cat. No.04CH37556).IEEE . Piscataway, NJ, USA*, pages pp.15–19.

[Seeger and Boser, 2003] Seeger, J. and Boser, B. (2003). Charge control of parallel-plate, electrostatic actuators and the tip-in instability. *Microelectromechanical Systems, Journal of*.

[Seeger and Boser, 2002] Seeger, J. I. and Boser, B. E. (2002). Parallel-plate driven oscillations and resonant pull-in. In *Solid-State Sensor, Actuator and Microsystems Workshop Hilton Head Island*.

[Seeger, 1997] Seeger, J.I. Crary, S. (1997). Stabilization of electrostatically actuated mechanical devices. *Solid State Sensors and Actuators, 1997. TRANSDUCERS '97*.

[Senturia, 2001] Senturia, S. (2001). *Microsystem Design*. Kluwer Acadenic Publishers, 1st edition.

[Shiba et al., 1998] Shiba, Y., Ono, T., Minami, K., and Esashi, M. (1998). Capacitive afm probe for high speed imaging. *ns. of the IEE of Japan*, 118 - E(12):647–650.

[Sung et al., 2000] Sung, S., Lee, J., Kang, T., and Song, J. W. (2000). Development of a tunable resonant accelerometer with self-sustained oscillation loop. In *IEEE National Aerospace and Electronics Conference*.

[Sung et al., 2003] Sung, S., Lee, J. G., and Kang, T. (2003). Development and test of mems accelerometer with self-sustatined oscillation loop. *Sensors and Actuators A*.

[Teymoori and Abbaspour-Sani, 2002] Teymoori, M. and Abbaspour-Sani, E. (2002). A novel electrostatic micromachined pump for drug delivery systems. In *Semiconductor Electronics, 2002. Proceedings. ICSE 2002. IEEE International Conference on*.

[Tilmans et al., 1999] Tilmans, H., Fullin, E., Ziad, H., van der Peer, M., Kesters, J., and al. (1999). A fully-packaged electromagnetic microrelay. *Micro Electro Mechanical Systems*.

[Tilmans and Legtenberg, 1994] Tilmans, H. A. C. and Legtenberg, R. (1994). Electrostatically driven vacuum-encapsulated polysilicon resonators part ii. theory and performance. *Sensors and Actuators A: Physical*.

[Tortonese et al., 1993] Tortonese, M., Barrett, R., and Quate, C. (1993). Atomic resolution with an atomic force microscope using piezoresistive detection. *Appl. Phys. Lett*, 62:8340–8363.

[Varghese et al., 1997] Varghese, M., Amantea, R., Sauer, D., and Senturia, S. D. (1997). Resistive damping of pulse-sensed capacitive position sensors. In *TRANSDUCERS '97, International Conference on Solid-state Sensors and Actuators*.

[Veijola et al., 1995] Veijola, T., Kuisma, H., Lahdenper, J., and Ryhnen, T. (1995). Equivalent-circuit model of the squeezed gas film in a silicon accelerometer. *Sensors and Actuators A: Physical*.

[Veijola and Turowski, 2001] Veijola, T. and Turowski, M. (2001). Compact damping models for laterally moving microstructures with gas-rarefaction effects. *Microelectromechanical Systems*.

[Vinokur, 2002] Vinokur, R. Y. (2002). Feasible analytical solutions for electrostatic parallel-plate actuator or sensor. *Journal of Vibration and Control*.

[Wang et al., 2004] Wang, X., Liu, Y., Wang, M., and Chen, X. (2004). The effect of air damping on the planar mems structures. In *HDP'04*.

[Wang et al., 1998] Wang, Y. C., Adams, S. G., Thorp, J. S., MacDonald, N. C., Hartwell, P., and Bertsch, F. (1998). Chaos in mems, parameter estimation and its potential application. *IEEE TRANSACTIONS ON CIRCUITS AND SYSTEMS*.

[Xie et al., 2003] Xie, W. C., Lee, H. P., and Lim, S. P. (2003). Nonlinear dynamic analysis of mems switches by nonlinear modal analysis. *Nonlinear Dynamics*, 31:243256.

[Yang and Senturia, 1996] Yang, Y. and Senturia, S. (1996). Numerical simulations of compressible squeezed-film damping. In *Solid-State Sensors and Actuators Workshop, Late News Session*.

[Yang et al., 1997] Yang, Y.-J., Gretillat, M.-A., and Senturia, S. (1997). Effect of air damping on the dynamics of nonuniform deformations of microstructures. *Solid State Sensors and Actuators, 1997. TRANSDUCERS '97*.

[YEH et al., 2001] YEH, B. Y., LIANG, Y. C., and TAY, F. E. H. (2001). Mathematical modelling on the quadrature error of low-rate microgyroscope for aerospace applications. *Analog Integrated Circuits and Signal Processing*.

[Younis et al., 2004] Younis, M. I., Abdel-Rahman, E., and Nayfeh, A. H. (2004). Global dynamics of mems resonators under superharmonic excitation. In *Proceedings of the 2004 International Conference on MEMS, NANO and Smart Systems*.

[Younis and Nayfeh, 2003] Younis, M. I. and Nayfeh, A. H. (2003). A study of the nonlinear response of a resonant microbeam to an electric actuation. *Nonlinear Dynamics*, 31:91117.

[Zhang et al., 2002] Zhang, W., Baskaran, R., and Turner, K. L. (2002). Effect of cubic nonlinearity on auto-parametrically amplified resonant mems mass sensor. *Sensors and Actuators A*.

[ZHAO et al., 2005] ZHAO, X., REDD, C. K., and NAYFEH, A. H. (2005). Nonlinear dynamics of an electrically driven impact microactuator. *Nonlinear Dynamics*.

[Zhou and Yang, 2003] Zhou, Y.-H. and Yang, X. (2003). Numerical analysis on snapping induced by electromechanical interaction of shuffling actuator with nonlinear plate. *Computers and Structures*.

[Zook et al., 1995] Zook, J., Burns, D., Herb, W., Guckel, H., Kang, J., and Ahn, Y. (1995). Optically excited self-resonant strain transducers. In *Transducers'95, 8th International Conference on Solid-State Sensors and Actuators*, volume 2.